Applied Numerical Mathematics 183 (2023) 236–262

Contents lists available at ScienceDirect

Applied Numerical Mathematics

www.elsevier.com/locate/apnum

A general vertical decomposition of Euler equations: Multilayer-moment models

J. Garres-Díaz [a], C. Escalante [b,*], T. Morales de Luna [c], M.J. Castro Díaz [c]

[a] Dpto. Matemáticas, Edificio Einstein - Universidad de Córdoba, Córdoba 14014, Spain
[b] Dpto. Matemática Aplicada, Universidad de Málaga, 29071 Málaga, Spain
[c] Dpto. Análisis Matemático, Estad. e I.O. y Matemática Aplicada, Universidad de Málaga, 29071 Málaga, Spain

ARTICLE INFO

Article history:
Received 5 May 2022
Received in revised form 23 July 2022
Accepted 9 September 2022
Available online 13 September 2022

Keywords:
Multilayer-moment models
Vertical discretizations
Shallow water flows
Free surface Euler equations

ABSTRACT

In this work, we present a general framework for vertical discretizations of Euler equations. It generalizes the usual moment and multilayer models and allows to obtain a family of multilayer-moment models. It considers a multilayer-type discretization where the layerwise velocity is a polynomial of arbitrary degree N on the vertical variable. The contribution of this work is twofold. First, we compare the multilayer and moment models in their usual formulation, pointing out some advantages/disadvantages of each approach. Second, a family of multilayer-moment models is proposed. As particular interesting case we shall consider a multilayer-moment model with layerwise linear horizontal velocity. Several numerical tests are presented, devoted to the comparison of multilayer and moment methods, and also showing that the proposed method with layerwise linear velocity allows us to obtain second order accuracy in the vertical direction. We show as well that the proposed approach allows to correctly represent the vertical structure of the solutions of the hydrostatic Euler equations. Moreover, the measured efficiency shows that in many situations, the proposed multilayer-moment model needs just a few layers to improve the results of the usual multilayer model with a high number of vertical layers.

© 2022 The Author(s). Published by Elsevier B.V. on behalf of IMACS. This is an open access article under the CC BY-NC-ND license (http://creativecommons.org/licenses/by-nc-nd/4.0/).

1. Introduction

The modeling and numerical simulation of geophysical flows is currently a very active topic of research. In particular, the study, analysis and numerical simulation of the well-known Navier-Stokes system [19] is of interest. It describes the motion of fluids and also can be employed for other complex geophysical flows as granular or debris flows.

Nevertheless, its complexity and specially the high computational cost associated to the resolution of this system makes that some other simpler approaches are usually proposed. One of the most widely used is the shallow-water (or Saint–Venant) system [21]. In the shallow water approach the characteristic length of the domain is assumed to be much longer than the vertical one, and then the vertical effects are assumed to be small when compared to the horizontal ones. Therefore, a vertical integration is done and the averaged horizontal velocity is considered. In [34] a rigorous derivation of this system, based on a asymptotic analysis, is introduced. This approach has been used in many recent works (see e.g. [9,35,4,49]).

* Corresponding author.
E-mail address: escalante@uma.es (C. Escalante).

https://doi.org/10.1016/j.apnum.2022.09.004
0168-9274/© 2022 The Author(s). Published by Elsevier B.V. on behalf of IMACS. This is an open access article under the CC BY-NC-ND license (http://creativecommons.org/licenses/by-nc-nd/4.0/).

Although shallow water type systems are quite popular, mainly due to the low computational cost required for their simulation, they present a main drawback: the vertical information is neglected. Indeed, considering the averaged horizontal velocity and neglecting the vertical deviations from this average leads us to lose important information for many practical applications. Several ways to overcome this limitation have been proposed in the literature. In next paragraphs we describe those that are relevant for our work.

A possible approach to capture vertical effects is to use the so-called σ-coordinate framework (see [50,17]). The idea is first to do a change of variables so that the vertical coordinates vary between 0, the bottom, and 1, the free surface. Then, the free surface is defined as a function of the horizontal coordinates which is derived from the standard kinematic free surface condition. The interval $[0, 1]$ is then discretized, giving a vertical approximation of the solution of the model. This approach has been used in [38,16,18,47] among others.

Another way to recover vertical effects in shallow flows is to use the so-called multilayer approach [3,6,30]. Multilayer systems consider a vertical division of the fluid into M given layers, where this division is not physical, but it may be considered as a virtual vertical discretization. Within each layer, a depth-averaged process is performed leading to a layerwise constant solution for the horizontal velocity. In [3] the vertical layers are immiscible, while [6,30] consider a mass and momentum transfer exchange between the internal layers. In recent years several works have been proposed based on this procedure to model fluids or complex geophysical flows such as bedload and suspension sediment transport, variable density flows or granular and debris flows (see [29,27,48,11,8,36,32,31] among others).

The last approach we describe here corresponds to the shallow water moment models [52,40]. In the moment approach, rather than dividing the vertical direction into layers, one single layer is considered, but now the variables are supposed to follow a polynomial profile, with an arbitrary degree of approximation, in the vertical direction. Again, this allows us to obtain vertical effects as now the horizontal velocity is not just a constant for the whole column of the fluid, but a polynomial on the vertical variable. We refer the reader to [45,41,43,12,33] among others for a better description and applications of this technique. An advantage of this approach with respect to the multilayer one is its lower computational cost. Typically, the vertical structure of solution could be capture more accurately with moment models with a low degree polynomial, while the number of layers required to obtain a similar solution with the multilayer approach demands more computational effort as it will be shown later on.

The contribution of this work is twofold. The first goal is to propose a common framework for vertical discretization of Euler equations, as well as a family of improved multilayer-moment methods. The idea is to avoid the usual difficulties and computational cost when solving the full 3D system, while keeping the information on the vertical direction with a low or moderate complexity and computational cost. The ideas proposed here not only can be seen as a generalization of the multilayer, σ-coordinate or moment approaches, but it will also allow us to generalize and propose new enriched models. In particular, we propose here a family of multilayer-moment method, based on this framework, to improve the accuracy of both methods, taking advantage of the strengths of each one.

The second objective will be to analyze the efficiency and accuracy of the different techniques. For instance, one may conjecture that the computational cost of moment method is lower than the multilayer one, specially when the number of layers M is large, since it increases in a quasi-linear way with M. However, moment method may not be enough to reproduce complex vertical profiles for the velocity. We aim to give answer to this conjecture and to do a thorough study of the efficiency, advantages and disadvantages of the different proposed approximations.

This paper is organized as follows: Section 2 is devoted to present the more general system considered here and its representation in σ-coordinates, which will be vertically discretized. In Section 3 we focus on the case of Euler system and we develop a vertical discretization to obtain the family of multilayer-moment models, and also analyze interesting particular cases. Section 4 is devoted to numerical test cases, and some conclusions are presented in Section 5. Finally, in appendixes Appendix A and Appendix B we give detail of how viscosity effects are included, as well as the particular cases of the classical multilayer and moment models.

2. Governing system

Let us start by establishing the system we are going to deal with. For the sake of simplicity, we consider here a two-dimensional flow, although everything might be generalized to the 3D case. Let (x, z) be the horizontal and normal directions, respectively, and $\boldsymbol{u} = (u, w)$ the velocity vector. Let us remark that, in this section, we do not necessarily fix a Cartesian reference system, but rather proceed in a general way. Therefore, the coordinates may be considered in a general reference system, for instance performing a rotation of Cartesian reference and using tilted coordinates, which may be useful in some applications such as gravity driven flows. The incompressible Navier-Stokes system for a fluid with constant density $\rho \in \mathbb{R}$ is given by

$$\begin{cases} \partial_x u + \partial_z w = 0, \\ \rho\big(\partial_t u + u\,\partial_x u + w\,\partial_z u\big) + \partial_x p = \rho f_x + \partial_x \tau_{xx} + \partial_z \tau_{xz}, \\ \rho\big(\partial_t w + u\,\partial_x w + w\,\partial_z w\big) + \partial_z p = \rho f_z + \partial_x \tau_{zx} + \partial_z \tau_{zz}, \end{cases} \tag{1}$$

where τ is the deviatoric stress tensor, p the pressure, and $f = (f_x, f_z)$ is the external force, usually representing the gravity force. For instance, if (x, z) are the usual Cartesian coordinates then $f = (0, -g)$. Other option is to consider a tilted reference system over a fixed inclined plane with slope $\theta > 0$, then $f = (g \sin\theta, -g\cos\theta)$.

We shall consider for now the decomposition of the pressure into hydrostatic and non-hydrostatic components:

$$p = \rho\,(p_H + p_{NH}), \quad \text{with} \quad \partial_z p_H = f_z.$$

We denote by $h(t, x)$ the fluid depth and we define $b(x)$ the bottom topography. We shall denote by $\eta(t, x) = h(t, x) + b(x)$ the free surface. As boundary conditions, we take the usual kinematic conditions at the bottom ($z = b$) and free surface ($z = \eta$):

$$u_{|z=b}\,\partial_x b = w_{|z=b}, \qquad \partial_t \eta + u_{|z=\eta}\,\partial_x \eta = w_{|z=\eta}.$$

In addition, we assume the usual normal stress balance at the free surface and a Darcy friction law at the bottom (see e.g. [33]):

$$\tau_{xz|z=b+h} = 0 \quad \text{and} \quad \tau_{xz|z=b} = \rho\epsilon\,\left|u_{|z=b}\right| u_{|z=b},$$

where ϵ is a dimensionless constant friction coefficient.

Now, we write system (1) in the so-called σ-coordinates. To this end, we consider the change of variable given by

$$\xi = \frac{z-b}{h}, \quad \text{where } \xi \in [0, 1] \text{ for } z \in [b, \eta].$$

Notice that $\xi = 0$ (respectively $\xi = 1$) corresponds to the bottom $z = b$ (respectively free surface $z = \eta$) level. Then, denoting by $\widetilde{\psi}(t, x, \xi) = \psi(t, x, \xi h + b)$, the differential operators read

$$\partial_\xi \widetilde{\psi} = h\partial_z \psi$$

and

$$h\partial_s \psi = \partial_s \left(h\widetilde{\psi}\right) - \partial_\xi \left(\partial_s\,(\xi h + b)\,\widetilde{\psi}\right), \qquad \text{for } s \in \{t, x\}.$$

Taking into account the new variables, the pressure is written as

$$\widetilde{p} = \rho\,(\widetilde{p}_H + \widetilde{p}_{NH}), \quad \text{with} \quad \partial_\xi \widetilde{p}_H = hf_z,$$

where it is clear that, assuming that the pressure is null at the surface, we obtain the expression for the hydrostatic pressure

$$\widetilde{p}_H = hf_z\,(\xi - 1).$$

Thus, the Navier-Stokes system in σ-coordinates reads

$$\begin{cases} \partial_x\,(h\widetilde{u}) + \partial_\xi\,(\widetilde{w} - \widetilde{u}\partial_x\,(\xi h + b)) = 0, \\ \partial_t\,(h\widetilde{u}) + \partial_x\left(h\widetilde{u}^2 + h\widetilde{p}_{NH}\right) - hf_z\partial_x\,(z_b + h) \\ \qquad -\partial_\xi\,(\omega\widetilde{u} - \widetilde{p}_{NH}\partial_x(h\xi + z_b)) = \partial_x(h\widetilde{\tau}_{xx}) + \partial_\xi\,(\widetilde{\tau}_{xz} - \widetilde{\tau}_{xx}\partial_x(h\xi + b)) \\ \partial_t\,(h\widetilde{w}) + \partial_x\,(h\widetilde{u}\widetilde{w}) - \partial_\xi\,(\omega\widetilde{w} + \widetilde{p}_{NH}) = \partial_x(h\widetilde{\tau}_{zx}) + \partial_\xi\,(\widetilde{\tau}_{zz} - \widetilde{\tau}_{zx}\partial_x(h\xi + b)), \end{cases} \tag{2a}$$

where by simplicity we consider here $\tau = \nu\left(\nabla\boldsymbol{u} + \nabla\boldsymbol{u}'\right)$, with $\nu = \mu/\rho$ a constant kinematic viscosity. In addition, $z_b = b + x\,f_x/f_z$ include all gravitational contributions, and ω corresponds to the vertical transference term written as

$$\omega(\xi) = \partial_t\,(h\xi + b) + \widetilde{u}(\xi)\partial_x\,(h\xi + b) - \widetilde{w}(\xi). \tag{2b}$$

Notice that we have used here $\widetilde{u^2} = \widetilde{u}^2$ and $\widetilde{uw} = \widetilde{u}\widetilde{w}$, and in the third equation of (2a) the hydrostatic pressure has been canceled with the external force.

As a simple case, we shall consider $\tau_{xz} = \nu\partial_z u$, ant then the boundary conditions are rewritten as

$$\begin{aligned} &\omega(0) = \widetilde{u}_{|\xi=0}\,\partial_x b - \widetilde{w}_{|\xi=0} = 0, \\ &\omega(1) = \partial_t \eta + \widetilde{u}_{|\xi=1}\,\partial_x \eta - \widetilde{w}_{|\xi=1} = 0, \end{aligned} \quad \text{and} \quad \begin{aligned} &\frac{\nu}{h}\left(\partial_\xi \widetilde{u}\right)_{|\xi=0} = \epsilon\,\left|\widetilde{u}_{|\xi=0}\right| \widetilde{u}_{|\xi=0}, \\ &\frac{\nu}{h}\left(\partial_\xi \widetilde{u}\right)_{|\xi=1} = 0. \end{aligned} \tag{2c}$$

In the following, for the sake of simplicity, we focus on the hydrostatic Euler system, and therefore the vertical momentum equation is replaced by the hydrostatic assumption and viscous effects are neglected. However, in the numerical test we will be interested on showing flows with vertical structure, which is produced by friction forces and vertical viscosity effects mainly. To do so, we eventually consider the vertical term $\partial_z \tau_{xz}$ in the model in usual multilayer and moment discretization, which has been already introduced in previous works and we detail it in Appendixes A and B.

3. A general vertical decomposition of Euler equations

In this section, we perform a vertical discretization for system (2). As we said in Section 1, the first main goal is to propose a general framework that generalizes the moment [45] and multilayer [30] approaches for shallow flows. Moreover, a family of models enhancing the vertical structure of the fluid is proposed.

For the sake of simplicity, let us assume for now that (x, z) are the Cartesian coordinates and therefore $f = (0, -g)^t$. Recall that $\eta = h + b$ denotes the free surface and we assume the pressure to be hydrostatic, $\widetilde{p} = gh(1-\xi)$. This means in practice that the equation for $\widetilde{w}$ is no longer considered, as $\widetilde{w}$ may be computed from the divergence free condition. Moreover, we shall neglect viscous terms for now, $\nu = 0$:

$$\begin{cases} \partial_x (h\widetilde{u}) + \partial_\xi (\widetilde{w} - \widetilde{u}\partial_x (\xi h + b)) = 0, \\ \partial_t (h\widetilde{u}) + \partial_x (h\widetilde{u}^2) + gh\partial_x \eta - \partial_\xi (\widetilde{u}\omega) = 0, \\ \omega = \partial_t (h\xi + b) + \widetilde{u}\partial_x (h\xi + b) - \widetilde{w}, \end{cases} \tag{3}$$

together with the kinematic conditions

$$\omega_{|\xi=0} = \omega_{|\xi=1} = 0.$$

In what follows we shall omit the notation $\widetilde{(\cdot)}$ and assume directly the dependence on (t, x, ξ). Moreover, using the definition of ω, the first equation in (3) is rewritten as

$$\partial_t h + \partial_x (hu) = \partial_\xi \omega, \tag{4}$$

which is integrated for $\xi \in [0, 1]$ to get

$$\partial_t h + \partial_x \left(h\overline{u}\right) = 0, \qquad \text{where} \qquad \overline{u} = \int_0^1 u d\xi. \tag{5}$$

In addition, using previous equations (4) and (5), we find an explicit expression, in terms of the spatial derivative, for the vertical transference term ω as

$$\omega_{|\xi} = \int_0^\xi (\partial_t h + \partial_x (hu))\, ds = -\xi \partial_x \left(h\overline{u}\right) + \partial_x \left(h \left(\int_0^\xi u(s) ds \right) \right) = \partial_x \left(h \left(\int_0^\xi u_{|\xi=s} ds - \xi \overline{u} \right) \right).$$

Notice that ω is continuous as long as u is an integrable function.

Thus, the σ-coordinate Euler equations (3) may be equivalently written as

$$\begin{cases} \partial_t h + \partial_x (hu) - \partial_\xi \omega = 0, \\ \partial_t (hu) + \partial_x (hu^2) + gh\partial_x \eta - \partial_\xi (u\omega) = 0, \\ \omega = \partial_x \left(h \left(\int_0^\xi u_{|\xi=s} ds - \xi \overline{u} \right) \right). \end{cases} \tag{6}$$

We consider now a vertical partition of the interval $[0, 1]$ into M layers, that is, we consider

$$0 = L_{1/2} < \cdots < L_{\alpha+1/2} < \cdots < L_{M+1/2} = 1,$$

and define $l_\alpha = L_{\alpha+1/2} - L_{\alpha-1/2} \in [0, 1]$, $\alpha = 1, \ldots, M$. Note that it holds then that

$$L_{\alpha+1/2} = \sum_{\beta=0}^{\alpha} l_\beta, \quad \alpha = 1, 2, \ldots, M, \qquad \text{and} \qquad L_{M+1/2} = \sum_{\alpha=1}^{M} l_\alpha = 1.$$

We shall define the layer Ω_α as

$$\Omega_\alpha = \{(x, \xi) \in \mathbb{R} \times [0, 1] : L_{\alpha-1/2} < \xi < L_{\alpha+1/2}\}, \qquad \text{for } \alpha = 1, \ldots, M.$$

Let U be a given general variable and consider its polynomial approximation within each layer:

$$U(t, x, \xi) = \sum_{\alpha=1}^{M} U_\alpha (t, x, \xi) \mathbb{1}_{\Omega_\alpha}(\xi), \text{ with } U_\alpha (t, x, \cdot) \in \mathbb{P}_N[\xi],$$

where $\mathbb{1}_{\Omega_\alpha}(\xi)$ is the characteristic function in the subdomain Ω_α. Consider now an orthogonal basis of $\mathbb{P}_N[\xi]$ in the interval $[0,1]$, consisting of the polynomials

$$\phi_j : [0,1] \to \mathbb{R},\ j = 0, 1, \dots, N,$$

and rescale them in the interval $[L_{\alpha-1/2}, L_{\alpha+1/2}]$, defining

$$\widehat{\phi}_{\alpha,j}(\xi) = \phi_j\left(\frac{\xi - L_{\alpha-1/2}}{l_\alpha}\right), \quad \xi \in [L_{\alpha-1/2}, L_{\alpha+1/2}].$$

We shall consider here the particular case of the Legendre polynomial basis, although any other choice could be made. In particular, the first polynomials of the basis are

$$\phi_0(\xi) = 1, \quad \phi_1(\xi) = 1 - 2\xi, \quad \phi_2(\xi) = 1 - 6\xi + 6\xi^2, \quad \phi_3(\xi) = 1 - 12\xi + 30\xi^2 - 20\xi^3.$$

Notice that these polynomials satisfy

$$\phi_i(0) = 1, \quad \text{and} \quad \int_0^1 \phi_i(\xi)\phi_j(\xi)\, d\xi = \mu_i \delta_{ij},$$

where δ_{ij} is the Kronecker symbol and μ_i is the square norm of ϕ_i in $\mathbb{P}_N[\xi]$, which is not necessarily 1 as the basis is assumed only to be orthogonal.

For the sake of generality, let us rewrite the system (6) as

$$\begin{cases} \partial_t h + \partial_x(hu) - \partial_\xi \omega = 0, & \text{(a)} \\ \partial_t U + \partial_x F(h,U) + \partial_\xi H(h,U) = S(h,U)\partial_x \eta, & \text{(b)} \\ \omega = \partial_x\left(h\left(\int_0^\xi u_{|_{\xi=s}} ds - \xi\overline{u}\right)\right), & \text{(c)} \end{cases} \tag{7}$$

with

$$U = hu, \quad F(h,U) = u\,U, \quad H(h,U,\omega) = -\frac{1}{h}\omega\, U, \quad S(h,U) = -gh.$$

Remark 1. Although in our case it is quite simple, since $U = hu$, writing the system in the form (7) allows us to consider any other generic variable. For instance, in the case of non-hydrostatic pressure it would be interesting to consider $U = (hu, hw)^t$ or in the presence of a passive scalar $c(t,x,\xi)$ transported by the fluid, we would use $U = (hu, hc)$. Therefore, the derivation performed in what follows will be as general as possible.

Let us denote by $\widehat{U}_{\alpha,j}$ the coordinates of $U_\alpha(t,x,\cdot)$ in the basis $\{\widehat{\phi}_{\alpha,j}\}_{j=0,\dots,N}$:

$$U_\alpha(t,x,\xi) = \sum_{j=0}^{N} \widehat{U}_{\alpha,j}(t,x)\widehat{\phi}_{\alpha,j}(\xi), \quad \text{for } \xi \in [L_{\alpha-1/2}, L_{\alpha+1/2}].$$

More explicitly, in our case we are considering $\widehat{U}_{\alpha,j} = h\widehat{u}_{\alpha,j}$.

We recall that, since the basis is orthogonal, we have

$$\int_{L_{\alpha-1/2}}^{L_{\alpha+1/2}} U_\alpha \widehat{\phi}_{\alpha,j}\, d\xi = l_\alpha \mu_j \widehat{U}_{\alpha,j}. \tag{8}$$

Let us introduce the following definitions, as they will be useful afterwards

$$A_{ijk} = \int_0^1 \phi_i\phi_j\phi_k d\xi, \quad B_{ijk} = \int_0^1 \phi_i'(\xi)\left(\int_0^\xi \phi_j(s)ds\right)\phi_k(\xi)d\xi, \quad C_{ijk} = \int_0^1 \phi_i'\phi_j\phi_k d\xi, \quad \mu_j = A_{0jj}$$

Remark 2.

$$A_{ij0} = \mu_j\delta_{ij}, \quad B_{0jk} = 0, \quad B_{ij0} = \phi_i(1)\mu_0\delta_{j0} - \mu_j\delta_{ij}, \quad C_{ijk} = C_{ikj}, \quad C_{0jk} = 0.$$

Moreover, it is easy to show that

$$\int_{L_{\alpha-1/2}}^{L_{\alpha+1/2}} \widehat{\phi}_i \widehat{\phi}_j \widehat{\phi}_k d\xi = \int_{L_{\alpha-1/2}}^{L_{\alpha+1/2}} (\phi_i \phi_j \phi_k)\left(\frac{\xi - L_{\alpha-1/2}}{l_\alpha}\right) d\xi = \int_0^1 (\phi_i \phi_j \phi_k)(s)\, l_\alpha ds = l_\alpha A_{ijk},$$

$$\int_{L_{\alpha-1/2}}^{L_{\alpha+1/2}} \widehat{\phi}_i'(\xi) \left(\int_{L_{\alpha-1/2}}^{\xi} \widehat{\phi}_j(s) ds \right) \widehat{\phi}_k(\xi) d\xi$$

$$= \int_{L_{\alpha-1/2}}^{L_{\alpha+1/2}} \frac{1}{l_\alpha} \phi_i'\left(\frac{\xi - L_{\alpha-1/2}}{l_\alpha}\right) \left(l_\alpha \int_0^{\frac{\xi - L_{\alpha-1/2}}{l_\alpha}} \phi_j(s) ds \right) \phi_k\left(\frac{\xi - L_{\alpha-1/2}}{l_\alpha}\right) d\xi$$

$$= l_\alpha \int_0^1 \phi_i'(s) \left(\int_0^s \phi_j(z)\, dz \right) \phi_k(s) ds = l_\alpha B_{ijk},$$

and

$$\int_{L_{\alpha-1/2}}^{L_{\alpha+1/2}} \widehat{\phi}_i' \widehat{\phi}_j \widehat{\phi}_k d\xi = \int_{L_{\alpha-1/2}}^{L_{\alpha+1/2}} \phi_i'\left(\frac{\xi - L_{\alpha-1/2}}{l_\alpha}\right) \frac{1}{l_\alpha} (\phi_j \phi_k)\left(\frac{\xi - L_{\alpha-1/2}}{l_\alpha}\right) d\xi = \int_0^1 (\phi_i' \phi_j \phi_k)(s) ds = C_{ijk}.$$

In the case of Legendre polynomials, we also have

$$\widehat{\phi}_j(L_{\alpha-1/2}) = \phi_j(0) = 1, \qquad \widehat{\phi}_j(L_{\alpha+1/2}) = \phi_j(1) = (-1)^j.$$

Let us remark that any other polynomial orthogonal basis could be used in principle. In case of changing the basis, then the coefficient $\mu_i, A_{ijk}, B_{ijk}, C_{ijk}$ must be accordingly modified.

In order to derive the final model, we first compute the mass conservation equation by integrating (7a). Afterwards we shall multiply the momentum equation (7b) by the basis functions $\widehat{\phi}_{\alpha,i}$ and perform a vertical integration in the layer. The integrated mass equation reads

$$l_\alpha \partial_t h + l_\alpha \partial_x \left(h \widehat{u}_{\alpha,0}\right) = \omega_{\alpha+1/2} - \omega_{\alpha-1/2}, \qquad \text{for } \alpha = 1, \dots, M, \tag{9}$$

where we have used that $\int_0^1 \phi_j d\xi = \delta_{j0}$. Summing the previous equations for $\alpha = 1, \dots, M$, or equivalently integrating the mass equation along the vertical domain $\xi \in [0, 1]$, we recover equation (5)

$$\partial_t h + \partial_x \left(h \overline{u}\right) = 0, \qquad \text{where} \qquad \overline{u} = \int_0^1 u\, d\xi = \sum_{\beta=1}^{M} l_\gamma\, \widehat{u}_{\beta,0}. \tag{10}$$

Moreover, using the expansion of U, the vertical transference term ω (7c), for $\xi \in [L_{\alpha-1/2}, L_{\alpha+1/2}]$, can be expressed as

$$\begin{aligned} \omega &= \sum_{\beta=1}^{\alpha-1} \partial_x \left(h \int_{L_{\beta-1/2}}^{L_{\beta+1/2}} u d\xi \right) + \partial_x \left(h \int_{L_{\alpha-1/2}}^{\xi} u d\xi \right) - \xi \partial_x \left(h \overline{u}\right) \\ &= \omega_{\alpha-1/2} + \left(L_{\alpha-1/2} - \xi\right) \partial_x \left(h \overline{u}\right) + \partial_x \left(h \int_{L_{\alpha-1/2}}^{\xi} u d\xi \right) \end{aligned} \tag{11}$$

with

$$\omega_{\alpha-1/2} = \sum_{\beta=1}^{\alpha-1} l_\beta\, \partial_x \left(h \left(\widehat{u}_{\beta,0} - \overline{u} \right) \right).$$

Let us focus now on the momentum equation (7b), which is multiplied by the basis function $\widehat{\phi}_{\alpha,i}$ and then integrated within each layer. We shall compute each term separately.

For the time derivative, from (8) we have

$$\int_{L_{\alpha-1/2}}^{L_{\alpha+1/2}} \partial_t U\, \widehat{\phi}_{\alpha,i}\, d\xi = l_\alpha\, \mu_i\, \partial_t \widehat{U}_{\alpha,i}. \tag{12}$$

The derivative of the convective flux yields

$$\begin{aligned}\int_{L_{\alpha-1/2}}^{L_{\alpha+1/2}} \partial_x F(h,U)\widehat{\phi}_{\alpha,i}\, d\xi &= \int_{L_{\alpha-1/2}}^{L_{\alpha+1/2}} \partial_x (u\,U)\widehat{\phi}_{\alpha,i}\, d\xi \\ &= \partial_x \left(\int_{L_{\alpha-1/2}}^{L_{\alpha+1/2}} \sum_{j,k=0}^{N} \widehat{u}_{\alpha,j}\widehat{U}_{\alpha,k}\widehat{\phi}_{\alpha,j}\widehat{\phi}_{\alpha,k}\widehat{\phi}_{\alpha,i}\, d\xi \right) = l_\alpha \sum_{j,k=0}^{N} A_{ijk}\partial_x \left(\widehat{u}_{\alpha,j}\widehat{U}_{\alpha,k}\right).\end{aligned} \tag{13}$$

The source term gives

$$\int_{L_{\alpha-1/2}}^{L_{\alpha+1/2}} S(h,U)\partial_x\eta\, \widehat{\phi}_{\alpha,i}\, d\xi = -gh\,\delta_{i0}\,\partial_x\eta. \tag{14}$$

Finally, the vertical transference term gives:

$$\int_{L_{\alpha-1/2}}^{L_{\alpha+1/2}} \partial_\xi H(h,U,\omega)\widehat{\phi}_{\alpha,i}\, d\xi = \phi_{\alpha,i}(1) H_{|_{\xi=L^-_{\alpha+1/2}}} - \phi_{\alpha,i}(0)\, H_{|_{\xi=L^+_{\alpha-1/2}}} - \int_{L_{\alpha-1/2}}^{L_{\alpha+1/2}} H(h,U,\omega)\widehat{\phi}'_{\alpha,i}\, d\xi. \tag{15}$$

In the particular case of the Legendre basis, we have $\phi_{\alpha,i}(1) = (-1)^i$ and $\phi_{\alpha,i}(0) = 1$. Let us further develop the last integral in (15) taking into account (11). Then,

$$\begin{aligned}\int_{L_{\alpha-1/2}}^{L_{\alpha+1/2}} H(h,U,\omega)\widehat{\phi}'_{\alpha,i}\, d\xi &= -\int_{L_{\alpha-1/2}}^{L_{\alpha+1/2}} \frac{1}{h}\omega U \widehat{\phi}'_{\alpha,i}\, d\xi \\ &= -\omega_{\alpha-1/2}\sum_{j=0}^{N}\frac{1}{h}\widehat{U}_{\alpha,j}\int_{L_{\alpha-1/2}}^{L_{\alpha+1/2}} \widehat{\phi}'_{\alpha,i}\widehat{\phi}_{\alpha,j}\, d\xi - \partial_x\left(h\overline{u}\right)\sum_{j=0}^{N}\frac{1}{h}\widehat{U}_{\alpha,j}\int_{L_{\alpha-1/2}}^{L_{\alpha+1/2}} \left(L_{\alpha-1/2}-\xi\right)\widehat{\phi}'_{\alpha,i}\widehat{\phi}_{\alpha,j}\, d\xi \\ &\quad - \sum_{j,k=0}^{N}\frac{1}{h}\widehat{U}_{\alpha,k}\partial_x(h\widehat{u}_{\alpha,j})\int_{L_{\alpha-1/2}}^{L_{\alpha+1/2}} \widehat{\phi}'_{\alpha,i}\left(\int_{L_{\alpha-1/2}}^{\xi} \widehat{\phi}_{\alpha,j}(s)ds\right)\widehat{\phi}_{\alpha,k}\, d\xi.\end{aligned}$$

Now, taking into account that

$$\int_{L_{\alpha-1/2}}^{L_{\alpha+1/2}} \left(L_{\alpha-1/2}-\xi\right)\widehat{\phi}'_{\alpha,i}\widehat{\phi}_{\alpha,j}\, d\xi = -l_\alpha \int_0^1 s\,\phi'_i(s)\phi_j(s)\, ds = -l_\alpha B_{i0j},$$

we have

$$\int_{L_{\alpha-1/2}}^{L_{\alpha+1/2}} H(h,U,\omega)\widehat{\phi}'_{\alpha,i} d\xi = -\omega_{\alpha-1/2}\sum_{j=0}^{N}\frac{1}{h}\widehat{U}_{\alpha,j}C_{ij0} + l_\alpha\partial_x\left(h\overline{u}\right)\sum_{j=0}^{N}\frac{1}{h}\widehat{U}_{\alpha,j}B_{i0j} - l_\alpha\sum_{j,k=0}^{N}\frac{1}{h}\widehat{U}_{\alpha,k}\partial_x(h\widehat{u}_{\alpha,j})B_{ijk}. \tag{16}$$

Combining (12), (13), (14), (15), and (16), for $\alpha = 1, 2, \ldots, M$ and $i = 0, 1, \ldots, N$, together with the mass equation (9), we get the final multilayer-moment system

$$\begin{cases} l_\alpha \partial_t h + l_\alpha \partial_x \left(h\widehat{u}_{\alpha,0}\right) = \omega_{\alpha+1/2} - \omega_{\alpha-1/2} \\ l_\alpha \mu_i \partial_t \widehat{U}_{\alpha,i} + l_\alpha \sum_{j,k=0}^{N} A_{ijk} \partial_x \left(\widehat{u}_{\alpha,j} \widehat{U}_{\alpha,k}\right) + gh\, \delta_{i0}\, e_1\, \partial_x \eta \\ \qquad = (-1)^i \dfrac{1}{h} (\omega U)_{|_{\xi = L^-_{\alpha+1/2}}} - \dfrac{1}{h} (\omega U)_{|_{\xi = L^+_{\alpha-1/2}}} \\ \qquad -\omega_{\alpha-1/2} \sum_{j=0}^{N} \dfrac{1}{h} \widehat{U}_{\alpha,j} C_{ij0} + l_\alpha \partial_x \left(h\overline{u}\right) \sum_{j=0}^{N} \dfrac{1}{h} \widehat{U}_{\alpha,j} B_{i0j} - l_\alpha \sum_{j,k=0}^{N} \dfrac{1}{h} \widehat{U}_{\alpha,k} \partial_x (h\widehat{u}_{\alpha,j}) B_{ijk}, \end{cases} \tag{17}$$

for $\alpha = 1, \dots, M$, where we recall that $\omega_{1/2} = \omega_{M+1/2} = 0$ and

$$\omega = \omega_{\alpha-1/2} + \left(L_{\alpha-1/2} - \xi\right) \partial_x \left(h\overline{u}\right) + \partial_x \left(h \int_{L_{\alpha-1/2}}^{\xi} u d\xi \right) \quad \text{with} \quad \omega_{\alpha-1/2} = \sum_{\beta=1}^{\alpha-1} l_\beta\, \partial_x \left(h \left(\widehat{u}_{\beta,0} - \overline{u}\right)\right).$$

Notice that the mass equation in previous system can be immediately replaced by (10).

Finally, a definition of $(\omega U)_{|_{\xi = L^\pm_{\alpha+1/2}}}$ is needed to close the system. Thanks to the continuity of ω we have

$$(\omega U)_{|_{\xi = L^\pm_{\alpha+1/2}}} = \omega_{\alpha+1/2}\, U_{|_{\xi = L^\pm_{\alpha+1/2}}} = \omega_{\alpha+1/2} U^\pm_{\alpha+1/2}$$

where here we must understand the limit values at the interfaces as

$$U^-_{\alpha+1/2} = \lim_{\substack{\xi \to L_{\alpha+1/2} \\ \xi < L_{\alpha+1/2}}} U_{|\Omega_\alpha} = \sum_{j=0}^{N} \widehat{U}_{\alpha,j} \widehat{\phi}_{\alpha,j}(L_{\alpha+1/2}) = \sum_{j=0}^{N} (-1)^j\, \widehat{U}_{\alpha,j},$$

$$U^+_{\alpha+1/2} = \lim_{\substack{\xi \to L_{\alpha+1/2} \\ \xi > L_{\alpha+1/2}}} U_{|\Omega_{\alpha+1}} = \sum_{j=0}^{N} \widehat{U}_{\alpha+1,j} \widehat{\phi}_{\alpha+1,j}(L_{\alpha+1/2}) = \sum_{j=0}^{N} \widehat{U}_{\alpha+1,j}.$$

Let us focus now on the particular case $U = hu$. We may now use a continuity argument at the interface for some particular combinations of the variable. This can be seen as an analogous procedure to what is done in [30], where jump conditions associated to the weak formulation of the original system are used. The detailed procedures are given in Appendix A. Then, after some straightforward computations, the term

$$u^-_{\alpha+1/2}\, \omega_{\alpha+1/2} - u^+_{\alpha-1/2}\, \omega_{\alpha-1/2}$$

in (15) is replaced by

$$\widetilde{u}_{\alpha+1/2}\, \omega_{\alpha+1/2} - \widetilde{u}_{\alpha-1/2}\, \omega_{\alpha-1/2} \tag{18}$$

where here $\widetilde{u}_{\alpha+1/2} = \left(u^+_{\alpha+1/2} + u^-_{\alpha+1/2}\right)/2$ is a centered approximation unless otherwise is specified (see Appendix A for details and in particular equation (A.4)).

Therefore, the final multilayer-moment system reads

$$\begin{cases} l_\alpha \partial_t h + l_\alpha \partial_x \left(h\widehat{u}_{\alpha,0}\right) = \omega_{\alpha+1/2} - \omega_{\alpha-1/2} \\ l_\alpha \mu_i \partial_t \left(h\widehat{u}_{\alpha,i}\right) + l_\alpha \sum_{j,k=0}^{N} A_{ijk} \partial_x \left(h\widehat{u}_{\alpha,j} \widehat{u}_{\alpha,k}\right) + gh\, \delta_{i0}\, e_1\, \partial_x \eta \\ \qquad = (-1)^i\, \widetilde{u}_{\alpha+1/2} \omega_{\alpha+1/2} - \widetilde{u}_{\alpha-1/2} \omega_{\alpha-1/2} \\ \qquad -\omega_{\alpha-1/2} \sum_{j=0}^{N} \widehat{u}_{\alpha,j} C_{ij0} + l_\alpha \partial_x \left(h\overline{u}\right) \sum_{j=0}^{N} \widehat{u}_{\alpha,j} B_{i0j} - l_\alpha \sum_{j,k=0}^{N} \widehat{u}_{\alpha,k} \partial_x (h\widehat{u}_{\alpha,j}) B_{ijk}, \end{cases}$$

for $\alpha = 1, \dots, M$.

In the most general case presented previously, we do not deal with viscous terms since they involve some essential and technical difficulties. Namely, derivatives in the stress tensor component when accounting for the discontinuities of the velocity profile at the internal interfaces have to be correctly defined. Moreover, when considering the case $M > 1, N > 0$ in the multilayer system with viscous terms, a usual discretization of such viscous terms does not ensure the convergence

of the system to the correct solution, and some techniques must be applied to overcome this problem (see e.g. [20,2]). All these difficulties are out of the scope of this paper, and it is currently a work in progress that will be studied in a forthcoming article. Nevertheless, this task is easier in some particular cases already introduced in the literature: see for instance the case of the usual multilayer (zero-moment case) and moment (one-layer case) models, which will be presented later.

Note that the previous system allows us to obtain a method that is expected to be $(N+1)$th order accurate in the vertical direction. Then, combining it with a high-order (horizontal) spatial reconstruction scheme (e.g. based on WENO operators) and a high order time integrator (e.g. Runge-Kutta), the resulting method is expected to be globally high-order.

Remark 3. Written in compact form, system (17) is equivalent to

$$\int_{L_{\alpha-1/2}}^{L_{\alpha+1/2}} \partial_t U \widehat{\phi}_{\alpha,i} d\xi + \int_{L_{\alpha-1/2}}^{L_{\alpha+1/2}} \partial_x F(h,U)\widehat{\phi}_{\alpha,i} d\xi - \int_{L_{\alpha-1/2}}^{L_{\alpha+1/2}} S(h,U)\partial_x \eta\, \widehat{\phi}_{\alpha,i} d\xi$$
$$+ \phi_{\alpha,i}(1) H_{|_{\xi=L^-_{\alpha+1/2}}} - \phi_{\alpha,i}(0)\, H_{|_{\xi=L^+_{\alpha-1/2}}} - \int_{L_{\alpha-1/2}}^{L_{\alpha+1/2}} H(h,U,\omega)\widehat{\phi}'_{\alpha,i} d\xi = 0.$$

This may be seen as a semi-discrete vertical discretization of (7) in the framework of the Discontinuous Galerkin (DG) methods. Note that the Legendre polynomials basis has largely been used in similar contexts, although one can find other different choices (see [52,40,22,23,44,53,43,41,12,7,33,42]). It is worth mentioning that, while the regular integrals are numerically approximated in other works (see for instance [24,37,26]), here we are computing those integrals exactly.

3.1. Particular cases

Let us consider now some particular cases of interest for (17). Concretely, we shall see that the proposed discretization gives the multilayer [30] and moment [45] models for particular choices of M and N, including the classical shallow water system. Finally, a new model is proposed, where the horizontal velocity is assumed to be linear within each vertical layer.

Shallow water system

The easiest case is when we only have a single layer ($M = 1$) and we use as polynomial approximation the constants ($N = 0$). Then, from system (17) we get

$$\partial_t h + \partial_x \left(h\widehat{u}_{1,0}\right) = \omega_{|_{\xi=1}} - \omega_{|_{\xi=0}},$$

and

$$\partial_t \widehat{U}_{1,0} + \partial_x \left(\widehat{u}_{1,0}\widehat{U}_{1,0}\right) + gh\partial_x\eta = \frac{1}{h}\left(\omega U\right)_{|_{\xi=1}} - \frac{1}{h}\left(\omega U\right)_{|_{\xi=0}}$$
$$- \omega_{|_{\xi=0}} \frac{1}{h}\widehat{U}_{1,0} C_{000} + \partial_x\left(h\overline{u}\right)\frac{1}{h}\widehat{U}_{1,0} B_{000} - \frac{1}{h}\widehat{U}_{1,0}\partial_x(h\widehat{u}_{1,0}) B_{000}.$$

Now using the fact that $B_{0jk} = 0$, $C_{0jk} = 0$, $\omega_{|_{\xi=1}} = \omega_{|_{\xi=0}} = 0$ and

$$\widehat{U}_{1,0} = \int_0^1 U d\xi = \overline{U} = h\overline{u},$$

then (17) gives us the classical shallow water system

$$\begin{cases} \partial_t h + \partial_x\left(h\overline{u}\right) = 0, \\ \partial_t\left(h\overline{u}\right) + \partial_x\left(h\overline{u}^2\right) + gh\partial_x\eta = 0. \end{cases}$$

Multilayer zero-moment case: multilayer constant system

We may consider now the case of M layers and constant polynomial approximation $N = 0$. In this case:

$$\begin{cases} l_\alpha \partial_t h + l_\alpha \partial_x \left(h\widehat{u}_{\alpha,0}\right) = \omega_{\alpha+1/2} - \omega_{\alpha-1/2} \\ l_\alpha \partial_t \widehat{U}_{\alpha,0} + l_\alpha \partial_x \left(\widehat{u}_{\alpha,0}\widehat{U}_{\alpha,0}\right) + gh\,\partial_x \eta \;=\; \dfrac{1}{h}\left(\omega U\right)_{|_{\xi=L^-_{\alpha+1/2}}} - \dfrac{1}{h}\left(\omega U\right)_{|_{\xi=L^+_{\alpha-1/2}}} \\ \qquad -\omega_{\alpha-1/2}\dfrac{1}{h}\widehat{U}_{\alpha,0}C_{000} + l_\alpha \partial_x \left(h\overline{u}\right)\dfrac{1}{h}\widehat{U}_{\alpha,0}B_{000} - l_\alpha \dfrac{1}{h}\widehat{U}_{\alpha,0}\partial_x(h\widehat{u}_{\alpha,0})B_{000}. \end{cases}$$

Taking into account now that $B_{0jk} = C_{0jk} = 0$, denoting the average within the layer by

$$\widehat{U}_{\alpha,0} = h\widehat{u}_{\alpha,0} = hu_\alpha,$$

and noticing that the definition of $\omega_{\alpha\pm1/2}$ coincides with the transference term through the layer interfaces in [30], i.e.,

$$\omega_{\alpha+1/2} = \sum_{\beta=1}^{\alpha} \partial_x \left(h\left(u_\beta - \overline{u}\right)\right), \quad \text{with} \quad \overline{u} = \sum_{\gamma=1}^{M} l_\gamma u_\gamma,$$

with $\omega_{1/2} = \omega_{M+1/2} = 0$, system (17) reduces to the multilayer system in [6,30]

$$\begin{cases} l_\alpha \left(\partial_t h + \partial_x \left(hu_\alpha\right)\right) = \omega_{\alpha+1/2} - \omega_{\alpha-1/2}, \\ l_\alpha \left(\partial_t \left(hu_\alpha\right) + \partial_x \left(hu_\alpha^2\right) + gh\partial_x \left(b+h\right)\right) = \widetilde{u}_{\alpha+1/2}\omega_{\alpha+1/2} - \widetilde{u}_{\alpha-1/2}\omega_{\alpha-1/2}, \end{cases} \tag{19}$$

for $\alpha = 1, \ldots, M$, where we consider here

$$\widetilde{u}_{\alpha+1/2} = \frac{u^-_{\alpha+1/2} + u^+_{\alpha+1/2}}{2} = \frac{u_\alpha + u_{\alpha+1}}{2}$$

unless otherwise stated (see Appendix A).

It is remarkable the fact that the derivation of multilayer models in this framework is simpler than the usual one, since the intermediate interfaces $L_{\alpha+1/2}$ depend no more on x, which simplifies the integration procedure.

Although the focus here is on Euler equations, it will be of interest including viscous or friction effects for some simulations. Therefore, for the sake of completeness, Appendix A.2 gives the main ideas on how these terms are included for the multilayer system.

Remark 4. In view of what has been said in Remark 3, the multilayer system [6,30] corresponds to a semi-discrete vertical discretization in the DG framework, where the polynomial space corresponds to constant functions, $u_{|\Omega_\alpha} \in \mathbb{P}_0[\xi]$.

Shallow water moment model

We now consider the case of one layer ($M = 1$) and arbitrary N, we get

$$\begin{cases} \partial_t h + \partial_x \left(h\widehat{u}_{1,0}\right) = \omega_{|_{\xi=1}} - \omega_{|_{\xi=0}}, \\ \mu_i \partial_t \widehat{U}_{1,i} + \displaystyle\sum_{j,k=0}^{N} A_{ijk}\partial_x \left(\widehat{u}_{1,j}\widehat{U}_{1,k}\right) + gh\,\delta_{i0}\,\partial_x \eta \\ \qquad = (-1)^i \dfrac{1}{h}\left(\omega U\right)_{|_{\xi=1}} - \dfrac{1}{h}\left(\omega U\right)_{|_{\xi=0}} \\ \qquad -\omega_{|_{\xi=0}} \displaystyle\sum_{j=0}^{N} \dfrac{1}{h}\widehat{U}_{1,j}C_{ij0} + \partial_x \left(h\overline{u}\right) \sum_{j=0}^{N} \dfrac{1}{h}\widehat{U}_{1,j}B_{i0j} - \sum_{j,k=0}^{N} \dfrac{1}{h}\widehat{U}_{1,k}\partial_x(h\widehat{u}_{1,j})B_{ijk}. \end{cases}$$

Now we use again that $B_{0jk} = 0$, $C_{0jk} = 0$, $\omega|_{\xi=0} = \omega|_{\xi=1} = 0$, the identity $A_{0jk} = \mu_j \delta_{jk} = \dfrac{\delta_{jk}}{2j+1}$, and

$$\widehat{U}_{1,0} = \int_0^1 U d\xi = h\widehat{u}_{1,0} = h\overline{u}.$$

Let us slightly simplify the notation by removing the subscript of the single layer, setting then

$$\widehat{U}_{1,i} = h\widehat{u}_{1,i} = h\widehat{u}_i,$$

the mass equation and the momentum for $i = 0$ takes the form

$$\partial_t h + \partial_x \left(h\overline{u}\right) = 0$$

$$\partial_t \left(h\widehat{u}_0\right) + \sum_{j=0}^{N} \partial_x \left(\frac{\widehat{u}_j^2}{2j+1}\right) + gh\,\partial_x \eta = 0.$$

For $i > 0$, we get

$$\mu_i \partial_t \left(h\widehat{u}_i\right) + \mu_i \partial_x \left(2h\widehat{u}_0\widehat{u}_i\right) + \sum_{j,k=1}^{N} A_{ijk}\partial_x \left(h\widehat{u}_j\widehat{u}_k\right) = \partial_x \left(h\widehat{u}_0\right) \sum_{j=0}^{N} \widehat{u}_j B_{i0j} - \sum_{j,k=0}^{N} \widehat{u}_k \partial_x (h\widehat{u}_j) B_{ijk}.$$

We look now the term on the right hand side,

$$\begin{aligned}
&\partial_x \left(h\widehat{u}_0\right) \sum_{j=0}^{N} \widehat{u}_j B_{i0j} - \sum_{j,k=0}^{N} \widehat{u}_k \partial_x (h\widehat{u}_j) B_{ijk} \\
&\qquad = \partial_x \left(h\widehat{u}_0\right) \sum_{j=0}^{N} \widehat{u}_j B_{i0j} - \sum_{k=0}^{N} \widehat{u}_k \partial_x (h\widehat{u}_0) B_{i0k} - \sum_{j=1}^{N} \widehat{u}_0 \partial_x (h\widehat{u}_j) B_{ij0} - \sum_{j,k=1}^{N} \widehat{u}_k \partial_x (h\widehat{u}_j) B_{ijk} \\
&\qquad\qquad = -\sum_{j=1}^{N} \widehat{u}_0 \partial_x (h\widehat{u}_j) B_{ij0} - \sum_{j,k=1}^{N} \widehat{u}_k \partial_x (h\widehat{u}_j) B_{ijk} \;=\; \mu_i \widehat{u}_0 \partial_x (h\widehat{u}_i) - \sum_{j,k=1}^{N} \widehat{u}_k \partial_x (h\widehat{u}_j) B_{ijk},
\end{aligned}$$

where the identity $B_{ij0} = \phi_i(1)\mu_0\delta_{j0} - \mu_j\delta_{ij}$ for $i > 0$ has been used. Thus, we obtain the usual writing of the inviscid shallow water moment model [45] with $i = 1, \ldots, N$:

$$\begin{cases}
\partial_t h + \partial_x \left(h\widehat{u}_0\right) = 0, \\
\partial_t \left(h\widehat{u}_0\right) + \partial_x \left(h\widehat{u}_0^2 + h\displaystyle\sum_{j=1}^{N} \frac{\widehat{u}_j^2}{2j+1}\right) + gh\,\partial_x \eta = 0, \\
\partial_t \left(h\widehat{u}_i\right) + \partial_x \left(2h\widehat{u}_0\widehat{u}_i + h\dfrac{1}{\mu_i} \displaystyle\sum_{j,k=1}^{N} A_{ijk}\widehat{u}_j\widehat{u}_k\right) = \widehat{u}_0 \partial_x (h\widehat{u}_i) - \dfrac{1}{\mu_i} \displaystyle\sum_{j,k=1}^{N} B_{ijk}\widehat{u}_k \partial_x (h\widehat{u}_j).
\end{cases} \tag{20}$$

Remark 5. In view of what has been said in Remark 3, the moment model [45] corresponds to a semi-discrete vertical discretization with a single element on the vertical direction, and the polynomial space corresponds to the Legendre polynomial basis of degree N, $u \in \mathbb{P}_N[\xi]$.

As in the multilayer case, we are going to perform some numerical tests involving viscous effects. Therefore, we give the details on how these terms are included in the moment model in Appendix B.

Multilayer first-moment case: multilayer linear system

From a practical point of view, and due to the complexity of the general system (17) from the numerical and implementation points of view, we will limit ourselves to the case M layers and $N = 1$, that is, a first order expansion of $U_\alpha(t, x, \cdot)$ inside of each vertical layer. The resulting model is a multilayer model where the velocity is linear on ξ at each layer:

$$U(t, x, \xi) = \sum_{\alpha=1}^{N} U_\alpha(t, x, \xi)\mathbb{1}_{\Omega_\alpha}(\xi), \quad \text{and} \quad U_\alpha(t, x, \xi) = \widehat{U}_{\alpha,0}(t, x) + \widehat{U}_{\alpha,1}(t, x)\widehat{\phi}_{\alpha,1}(\xi).$$

In this case, the coefficients appearing in the system are

$$A_{0jk} = \mu_j\delta_{jk}, \quad A_{100} = A_{111} = 0, \quad A_{110} = A_{101} = \mu_1 = \frac{1}{3},$$

$$C_{0ij} = B_{0ij} = 0, \quad C_{100} = -2, \quad C_{110} = 0,$$

$$B_{100} = -1, \quad B_{101} = \mu_1, \quad B_{110} = -\mu_1, \quad B_{111} = 0,$$

and the moment equation for $i = 1$ is

$$
\begin{aligned}
l_\alpha \mu_1 \partial_t \widehat{U}_{\alpha,1} + l_\alpha \mu_1 \partial_x \left(\widehat{u}_{\alpha,0}\widehat{U}_{\alpha,1} + \widehat{u}_{\alpha,1}\widehat{U}_{\alpha,0}\right) &= -\frac{1}{h}\left(\omega U\right)_{|_{\xi=L^-_{\alpha+1/2}}} - \frac{1}{h}\left(\omega U\right)_{|_{\xi=L^+_{\alpha-1/2}}} \\
&-\omega_{\alpha-1/2}\frac{1}{h}\widehat{U}_{\alpha,0}(-2) + l_\alpha \partial_x\left(h\overline{u}\right)\frac{1}{h}\left(\widehat{U}_{\alpha,0}(-1) + \widehat{U}_{\alpha,1}\mu_1\right) \\
&-l_\alpha \frac{1}{h}\left(\widehat{U}_{\alpha,0}(-1) + \widehat{U}_{\alpha,1}\mu_1\right)\partial_x(h\widehat{u}_{\alpha,0}) - l_\alpha \frac{1}{h}\widehat{U}_{\alpha,0}\left(-\mu_1\right)\partial_x(h\widehat{u}_{\alpha,1}).
\end{aligned}
$$

Let us rewrite the term involving coefficient B_{1ij}, C_{1ij} as

$$
\begin{aligned}
&l_\alpha \mu_1 \frac{1}{h}\widehat{U}_{\alpha,0}\partial_x(h\widehat{u}_{\alpha,1}) + 2\omega_{\alpha-1/2}\frac{1}{h}\widehat{U}_{\alpha,0} + \frac{1}{h}\left(\widehat{U}_{\alpha,0} - \mu_1\widehat{U}_{\alpha,1}\right)\left(\omega_{\alpha+1/2} - \omega_{\alpha-1/2}\right) \\
&= l_\alpha \mu_1 \frac{1}{h}\widehat{U}_{\alpha,0}\partial_x(h\widehat{u}_{\alpha,1}) + \frac{1}{h}\left(\widehat{U}_{\alpha,0} - \mu_1\widehat{U}_{\alpha,1}\right)\omega_{\alpha+1/2} + \frac{1}{h}\left(\widehat{U}_{\alpha,0} + \mu_1\widehat{U}_{\alpha,1}\right)\omega_{\alpha-1/2}.
\end{aligned}
$$

Then, the final system, for $\alpha = 1, \dots, M$, reads

$$
\begin{cases}
l_\alpha \partial_t h + l_\alpha \partial_x\left(h\widehat{u}_{\alpha,0}\right) = \omega_{\alpha+1/2} - \omega_{\alpha-1/2}, \\[2ex]
l_\alpha \partial_t \widehat{U}_{\alpha,0} + l_\alpha \partial_x\left(\widehat{u}_{\alpha,0}\widehat{U}_{\alpha,0} + \mu_1\widehat{u}_{\alpha,1}\widehat{U}_{\alpha,1}\right) + gh\partial_x\eta = \frac{1}{h}\left(\omega U\right)_{|_{\xi=L^-_{\alpha+1/2}}} - \frac{1}{h}\left(\omega U\right)_{|_{\xi=L^+_{\alpha-1/2}}}, \\[2ex]
l_\alpha \mu_1 \partial_t \widehat{U}_{\alpha,1} + l_\alpha \mu_1 \partial_x\left(\widehat{u}_{\alpha,0}\widehat{U}_{\alpha,1} + \widehat{u}_{\alpha,1}\widehat{U}_{\alpha,0}\right) = -\frac{1}{h}\left(\omega U\right)_{|_{\xi=L^-_{\alpha+1/2}}} - \frac{1}{h}\left(\omega U\right)_{|_{\xi=L^+_{\alpha-1/2}}} \\
\qquad + l_\alpha \mu_1 \frac{1}{h}\widehat{U}_{\alpha,0}\partial_x(h\widehat{u}_{\alpha,1}) + \frac{1}{h}\left(\widehat{U}_{\alpha,0} - \mu_1\widehat{U}_{\alpha,1}\right)\omega_{\alpha+1/2} + \frac{1}{h}\left(\widehat{U}_{\alpha,0} + \mu_1\widehat{U}_{\alpha,1}\right)\omega_{\alpha-1/2}.
\end{cases}
$$

Finally, let us set the system involving just the horizontal velocity, and the mass equation obtained when summing all the layers

$$
\begin{cases}
\partial_t h + l_\alpha \partial_x\left(h\sum_{\alpha=1}^{M}\widehat{u}_{\alpha,0}\right) = 0, \\[2ex]
l_\alpha \partial_t\left(h\widehat{u}_{\alpha,0}\right) + l_\alpha \partial_x\left(h\widehat{u}^2_{\alpha,0} + \frac{h\widehat{u}^2_{\alpha,1}}{3}\right) + gh\partial_x\eta = \omega_{\alpha+1/2}\widetilde{u}_{\alpha+1/2} - \omega_{\alpha-1/2}\widetilde{u}_{\alpha-1/2}, \\[2ex]
l_\alpha \mu_1 \partial_t\left(h\widehat{u}_{\alpha,1}\right) + l_\alpha \mu_1 \partial_x\left(2h\widehat{u}_{\alpha,0}\widehat{u}_{\alpha,1}\right) = -\omega_{\alpha+1/2}\widetilde{u}_{\alpha+1/2} - \omega_{\alpha-1/2}\widetilde{u}_{\alpha-1/2} \\
\qquad + l_\alpha \mu_1 \widehat{u}_{\alpha,0}\partial_x(h\widehat{u}_{\alpha,1}) + \left(\widehat{u}_{\alpha,0} - \mu_1\widehat{u}_{\alpha,1}\right)\omega_{\alpha+1/2} + \left(\widehat{u}_{\alpha,0} + \mu_1\widehat{u}_{\alpha,1}\right)\omega_{\alpha-1/2},
\end{cases}
\tag{21}
$$

for $\alpha = 1, \dots, M$, where

$$
\widetilde{u}_{\alpha+1/2} = \frac{u^-_{\alpha+1/2} + u^+_{\alpha+1/2}}{2} = \frac{\widehat{u}_{\alpha,0} + \widehat{u}_{\alpha+1,0}}{2} + \frac{\widehat{u}_{\alpha+1,1} - \widehat{u}_{\alpha,1}}{2}
$$

unless otherwise stated (see Appendix A).

Remark 6. One should note that a loss of hyperbolicity could arise in certain situations, although we have not found difficulties in this sense for the practical applications shown here. Indeed, it is a known fact that the shallow water (one layer $M = 1$) moment system is hyperbolic for the first-order case ($N = 1$), but the same does not hold for the case $N > 1$. This fact is studied in [42], where authors introduced two alternative families of hyperbolic shallow water moment models, denoted there as Hyperbolic Shallow Water Moment and β-Hyperbolic Shallow Water Moment. They correspond to small modifications of the non-conservative terms in the original Shallow Water Moment system.

Moreover, in the case of multilayer system ($N = 0$), the hyperbolicity of multilayer systems is only proven for the two-layer case (see [6]). In contrast, a linearization process was performed in [31] which concluded that hyperbolicity may be lost when there is a big difference between layer velocities and the global average velocity.

Therefore one expects that hyperbolicity may be lost in the general case of multilayer moment model system.

4. Numerical results

We present in this section some numerical tests showing an interesting comparison between multilayer and moment models. Firstly we perform a simple test including viscosity and friction force to have diversity in the velocity profiles. Next, some more tests in the inviscid case are performed to include also the results of the first order multilayer-moment model derived in Subsection 3.1.

In the next subsections, we perform two families of tests. First, subsections 4.1 and 4.2 aim to give a comparison between usual multilayer (A.5) and moment models (B.1) commonly used, in particular in the viscous case to obtain a natural vertical structure. Concerning the numerical scheme, we have carried out the simulation using a standard first order path-conservative HLL finite volume scheme as described in [15]. Let us remark that when viscous terms are included in the standard multilayer and moment models, a semi-implicit discretization is used (see, e.g. [28] and [33] for the multilayer and moment systems, respectively) in order to avoid any restrictive time-step condition.

Second, subsections 4.3 and 4.4 show the convergence of the multilayer models with constant (zero-moment) (19) and linear (first-moment) (21) horizontal velocity to stationary solutions of hydrostatic Euler equations, as well as an accuracy test. For those tests, we consider a second order path-conservative HLL scheme based on a MUSCL reconstruction [14].

In order to construct the HLL scheme, we follow [15] with the following minimum (λ_1) and maximum (λ_2) wave speeds:

- Shallow water moment model:

$$\lambda_1 = \widehat{u}_0 - \sqrt{gh + \widehat{u}_1^2}, \qquad \lambda_2 = \widehat{u}_0 + \sqrt{gh + \widehat{u}_1^2}.$$

- Multilayer constant system:

$$\lambda_1 = \overline{u} - \sqrt{gh}, \qquad \lambda_2 = \overline{u} + \sqrt{gh}.$$

- Multilayer linear system:

$$\lambda_1 = \overline{u} - \sqrt{gh + \overline{u}_1^2}, \qquad \lambda_2 = \overline{u} + \sqrt{gh + \overline{u}_1^2},$$

with

$$\overline{u} = \sum_{\alpha=1}^{M} l_\alpha \widehat{u}_{\alpha,0} \qquad \text{and} \qquad \overline{u}_1 = \sum_{\alpha=1}^{M} l_\alpha \widehat{u}_{\alpha,1}.$$

Remark that, although the hyperbolicity of the systems is not proven as explained in Remark 6, we do not find any practical problem related to this aspect in the presented numerical tests. Remark also that there are no wet/dry areas in the considered tests. In such a case, any of the standard techniques dealing with this problem (see [13,46,25,51] among many others) could be applied.

Let us mention that one could make this method more efficient by using some strategies as the ones developed for multilayer and DG discretizations. In particular, a locally variable (in the spacial direction) number of vertical layers (see e.g. [31]) and/or polynomial degree for the moment description (see e.g. [1]) could be used. Moreover, both strategies could be employed at the same time to construct efficient and flexible methods, especially for realistic applications. However, this is out of the scope of this paper.

4.1. Multilayer and moment model in subcritical viscous flow

Here we compare the results of the standard multilayer and moment models in a viscous subcritical flow. The viscous and friction forces generate complex and different velocity profiles along the domain, from almost constant to parabolic profiles and recirculations in the flow. This test aims to show how multilayer and moment models reproduce these profiles and explore each approach's limitations and advantages/disadvantages. To this aim, we consider as a reference solution the one obtained with a very fine discretization computed by the multilayer model with 640 vertical layers.

We consider a classical subcritical test in a domain $x \in [-25, 25]$, where the initial free surface and discharge are $\eta(x) = 5$ m and $q(x) = 4.42$ m^2/s respectively, and the bottom is

$$b(x) = \begin{cases} 0.05 - 0.001x + 2\cos^2\left(\dfrac{\pi x}{10}\right) \text{ m} & \text{if } |x| < 5, \\ 0.05 - 0.001x \text{ m} & \text{otherwise.} \end{cases}$$

We use 200 point in the horizontal discretization, with CFL $= 0.8$, and subcritical boundary conditions (inlet discharge $q_{in} = 4.42$ m^2/s and outlet free surface $\eta_{out} = 5$ m). The final time is $t_f = 1000$ s. We show the results for a low ($\nu = 0.001$ m^2/s) and high kinematic viscosity ($\nu = 1$ m^2/s) case, with strong friction $\epsilon = 100\nu$. For each case we show the approximation of the free surface and the errors made by the moment and the multilayer approaches. To this aim, we shall measure relative errors as follows:

Consider an horizontal discretization of the domain $I = [a, b]$ by means of N_x volumes of constant size $\Delta x = \dfrac{b-a}{N_x}$,

$$I_i = [x_{i-1/2}, x_{i+1/2}], \qquad \text{for } i = 1, 2, \ldots, N_x,$$

where $x_{1/2} = a$, and $x_{i+1/2} = x_{i-1/2} + \Delta x$ for $i = 1, 2, \ldots, N_x$. We will denote as well $x_i = \dfrac{x_{i-1/2} + x_{i+1/2}}{2}$ the center of the cell I_i.

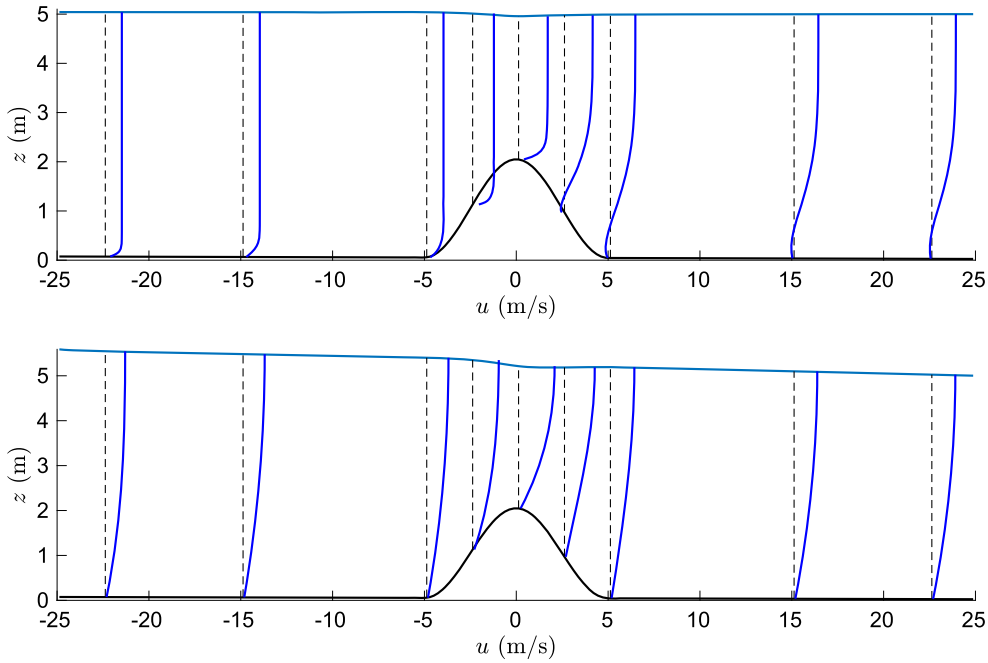

Fig. 1. Steady state solution for low ($\nu = 0.001$ m^2/s, upper figure) and high ($\nu = 1$ m^2/s, lower figure) viscosity cases. Blue lines correspond to the vertical profiles of velocity at locations $x = -22.5, -15, -5, -2.5, 0, 2.5, 5, 15, 22.5$ m. (For interpretation of the colors in the figure(s), the reader is referred to the web version of this article.)

Consider as well a vertical partition of the interval $[0, 1]$ into M layers

$$0 = L_{1/2} < \cdots < L_{\alpha+1/2} < \cdots < L_{M+1/2} = 1.$$

For any generic variable v denote by $v_{\alpha,i}$ the approximation obtained for v in the cell i and layer α. Then we shall denote by

$$\|v\|_2 = \sqrt{\Delta x \sum_{i=1}^{N_x} \frac{h_i}{M} \sum_{\alpha=1}^{M} v_{\alpha,i}^2}, \qquad \text{and} \qquad \|v\|_\infty = \max_{\substack{\alpha=1,\dots,M \\ i=1,\dots,N_x}} \left| v_{\alpha,i} \right|.$$

Remark that in the particular case that v does not depend on the vertical variable ξ, then we simply consider $v_{\alpha,i} \equiv v_i$ for $\alpha = 1, \dots, M$. We then compute the relative errors by

$$\mathrm{Err}_p[v] = \frac{\|v - \widetilde{v}^{ref}\|_p}{\|\widetilde{v}^{ref}\|_p}, \quad \text{for } p = 2, \infty,$$

where $\widetilde{v}^{ref}$ is a given reference solution.

We will be interested as well in computing the errors in the vertical direction for a given cell I_i, so that we denote by

$$\|v\|_{I_i,2} = \sqrt{\frac{h_i}{M} \sum_{\alpha=1}^{M} v_{\alpha,i}^2}, \qquad \text{and} \qquad \|v\|_{I_i,\infty} = \max_{\alpha=1,\dots,M} \left| v_{\alpha,i} \right|,$$

and we compute the relative errors

$$\mathrm{Err}_p^z[v, x_i] = \frac{\|v - \widetilde{v}^{ref}\|_{I_i,p}}{\|\widetilde{v}^{ref}\|_{I_i,p}}, \quad \text{for } p = 2, \infty.$$

Here, the solution of the multilayer model, obtained with 700 nodes and 640 vertical layers, will be considered as the reference solution. Then, when computing the errors, $\widetilde{v}^{ref}$ should be understood as the projection of the reference solution onto the space of the local solution v. For the case of moment models, the vertical velocity profile is computed, and its value at the center of the corresponding layer is obtained for the errors.

In Fig. 1 we see the steady state solution reached by both approaches for the free surface at the final time for both considered values of the viscosity, together with vertical profiles of the velocity at some particular locations. On the one

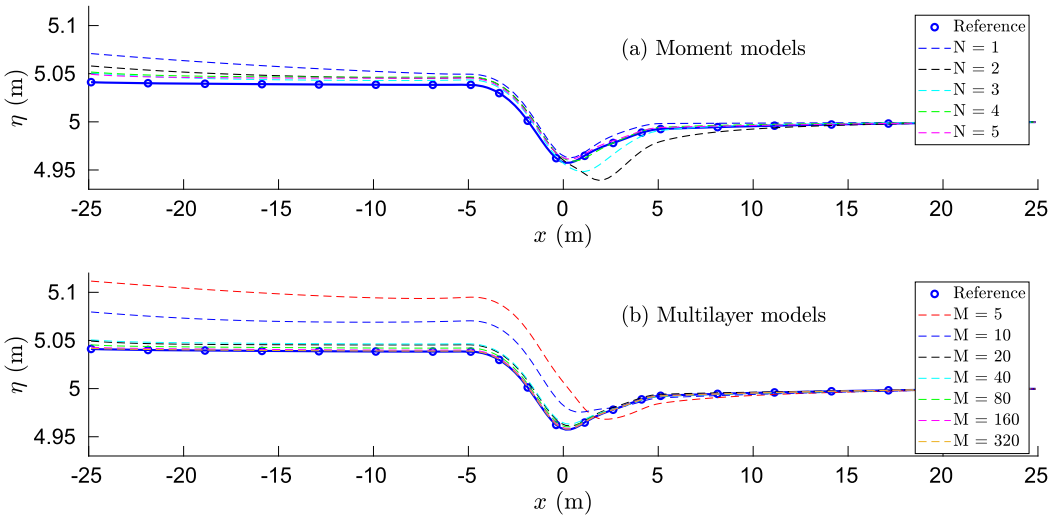

Fig. 2. Free surface approximation with moment and multilayer models for the low viscosity case.

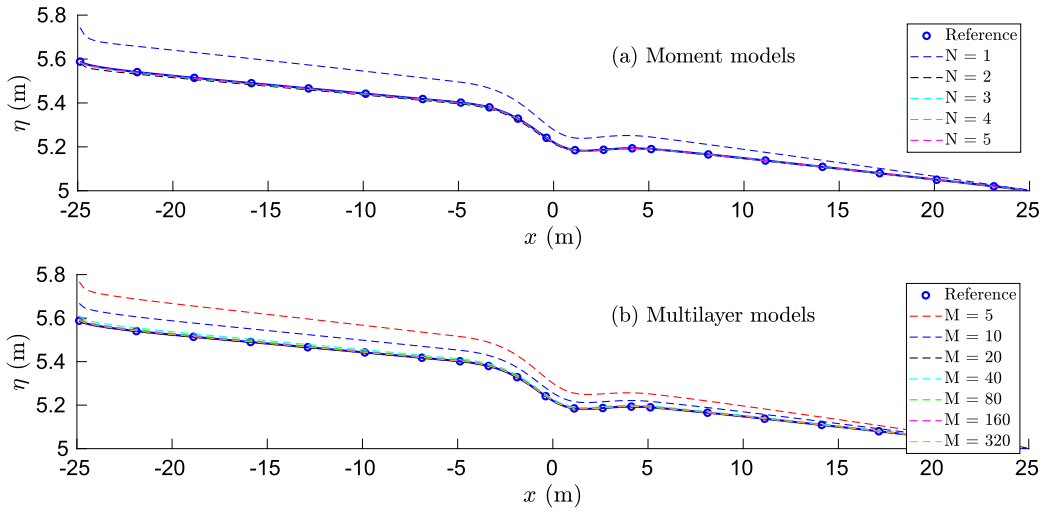

Fig. 3. Free surface approximation with moment and multilayer models for the high viscosity case.

hand, in the low viscosity case (upper figure) and for the first half of the domain, the velocity profile is almost a straight profile except near the bottom, where the velocity is smaller due to the friction force. However, the velocity profile is more complex after the bump, and we find recirculation areas (change on the sign of the velocity along the vertical direction) near the bottom. On the other hand, for the high viscosity case (lower figure), the velocity follows a parabolic profile along the whole domain.

Figs. 2 and 3 show the free surface computed with both the multilayer and moment approach, and Tables 1 and 2 show the relative errors made on the free surface, averaged velocity and the full velocity field, measured with respect to the reference solution. In Fig. 2 we see the convergence to the reference solution in the multilayer case. In the case of moment models, although the convergence towards the reference solution is not fully obtained for $N = 5$, especially in the left region. That is due to the fact that the vertical profiles of velocity are straight lines almost everywhere in the vertical direction, and moment models do not properly reproduce these profiles, as we discuss later. Nevertheless, we see that the errors made by the moment models are of the same order of magnitude as the multilayer models. Actually, we see that the errors made by the multilayer model with 20 layers and the 2nd order moment model are similar, while the computational cost for the former is much bigger than for the latter. Moreover, to improve the 5th order moment model results, we need to use 80 layers in the multilayer system. The computational effort for both approaches is shown in Fig. 4, where we see that moment models are cheaper than multilayer models from the computational point of view.

Fig. 3 and Table 2 show the results for the high viscosity case, where the vertical profile of velocity is approximately a parabolic profile along the whole domain. Looking at Fig. 3, we observe that there is convergence to the reference solution

Table 1
Relative errors in the low viscosity case made on the free surface (η), averaged velocity ($\overline{u}$) and the velocity field ($u = u(x, z)$) by the multilayer models (M layers) and the moment models (order N).

	$\mathrm{Err}_2\ [\eta]$	$\mathrm{Err}_2\ [\overline{u}]$	$\mathrm{Err}_2\ [u]$	$\mathrm{Err}_\infty\ [\eta]$	$\mathrm{Err}_\infty\ [\overline{u}]$	$\mathrm{Err}_\infty\ [u]$
M			Multilayer	(M layers)		
5	8.57×10^{-3}	1.04×10^{-2}	2.63×10^{-1}	1.39×10^{-2}	1.94×10^{-2}	5.24×10^{-1}
10	4.58×10^{-3}	5.65×10^{-3}	1.81×10^{-1}	7.61×10^{-3}	1.04×10^{-2}	4.40×10^{-1}
20	2.44×10^{-3}	3.05×10^{-3}	1.07×10^{-1}	4.01×10^{-3}	5.51×10^{-3}	3.42×10^{-1}
40	1.13×10^{-3}	1.46×10^{-3}	5.27×10^{-2}	1.86×10^{-3}	2.58×10^{-3}	2.03×10^{-1}
80	5.17×10^{-4}	6.89×10^{-4}	2.45×10^{-2}	8.47×10^{-4}	1.20×10^{-3}	1.08×10^{-1}
160	2.22×10^{-4}	3.07×10^{-4}	1.06×10^{-2}	3.63×10^{-4}	5.34×10^{-4}	5.60×10^{-2}
320	7.44×10^{-5}	1.06×10^{-4}	3.54×10^{-3}	1.21×10^{-4}	1.83×10^{-4}	2.27×10^{-2}
N			Moment	(order N)		
1	2.65×10^{-3}	2.93×10^{-3}	2.09×10^{-1}	5.88×10^{-3}	3.63×10^{-3}	4.38×10^{-1}
2	2.10×10^{-3}	2.86×10^{-3}	1.62×10^{-1}	6.90×10^{-3}	7.33×10^{-3}	4.14×10^{-1}
3	1.04×10^{-3}	1.66×10^{-3}	1.18×10^{-1}	3.66×10^{-3}	4.84×10^{-3}	3.64×10^{-1}
4	1.15×10^{-3}	1.45×10^{-3}	8.11×10^{-2}	2.09×10^{-3}	2.60×10^{-3}	2.77×10^{-1}
5	9.63×10^{-4}	1.23×10^{-3}	5.42×10^{-2}	1.61×10^{-3}	2.19×10^{-3}	1.94×10^{-1}

Table 2
Relative errors in the high viscosity case made on the free surface (η), averaged velocity ($\overline{u}$) and the velocity field ($u = u(x, z)$) by the multilayer models (M layers) and the moment models (order N).

	$\mathrm{Err}_2\ [\eta]$	$\mathrm{Err}_2\ [\overline{u}]$	$\mathrm{Err}_2\ [u]$	$\mathrm{Err}_\infty\ [\eta]$	$\mathrm{Err}_\infty\ [\overline{u}]$	$\mathrm{Err}_\infty\ [u]$
M			Multilayer	(M layers)		
5	1.83×10^{-2}	3.79×10^{-2}	1.23×10^{-1}	3.19×10^{-2}	4.63×10^{-2}	1.85×10^{-1}
10	8.13×10^{-3}	1.81×10^{-2}	5.62×10^{-2}	1.42×10^{-2}	2.19×10^{-2}	1.30×10^{-1}
20	3.82×10^{-3}	8.50×10^{-3}	2.65×10^{-2}	6.63×10^{-3}	1.04×10^{-2}	8.79×10^{-2}
40	1.81×10^{-3}	3.95×10^{-3}	1.25×10^{-2}	3.14×10^{-3}	4.83×10^{-3}	5.16×10^{-2}
80	8.40×10^{-4}	1.79×10^{-3}	5.79×10^{-3}	1.45×10^{-3}	2.20×10^{-3}	2.68×10^{-2}
160	3.58×10^{-4}	7.56×10^{-4}	2.47×10^{-3}	6.18×10^{-4}	9.32×10^{-4}	1.22×10^{-2}
320	1.19×10^{-4}	2.50×10^{-4}	8.21×10^{-4}	2.06×10^{-4}	3.08×10^{-4}	4.18×10^{-3}
N			Moment	(order N)		
1	1.49×10^{-2}	3.98×10^{-2}	1.49×10^{-1}	2.76×10^{-2}	4.72×10^{-2}	2.81×10^{-1}
2	1.05×10^{-3}	9.67×10^{-3}	2.30×10^{-2}	2.57×10^{-3}	1.31×10^{-2}	1.14×10^{-1}
3	4.27×10^{-4}	4.26×10^{-3}	8.28×10^{-3}	1.16×10^{-3}	5.62×10^{-3}	7.77×10^{-2}
4	2.54×10^{-4}	1.79×10^{-3}	3.98×10^{-3}	6.24×10^{-4}	2.34×10^{-3}	4.87×10^{-2}
5	1.79×10^{-4}	6.65×10^{-4}	2.12×10^{-3}	3.74×10^{-4}	8.60×10^{-4}	2.83×10^{-2}

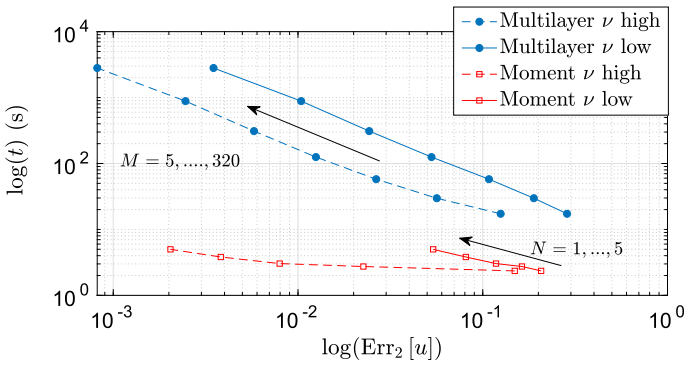

Fig. 4. Wall-clock time compared to L^2 errors on the velocity field, in log scale, for multilayer and moment models.

for free surface. It can be stated that the errors for the moment models appearing in Table 2 are smaller than in the previous case, in particular for the velocity field. That is due to the better approximation of the velocity profile along the domain since they are close to a parabolic profile, which is well approximated by polynomials and, therefore, by the moment approach. Note that in this case, the 3rd order moment model improves the results of the multilayer model with 40 layers, and the 5th order moment model produces smaller errors than the multilayer model with 160 layers.

That is an interesting result since the computational time increases fast with the number of layers. This can be seen in Table 3, where we show the ratios between the elapsed times for the multilayer models and the 3rd, 4th and 5th order moment models, obtained when simulating up to the final time $t_f = 1000$ s. We see for instance that the 5th order moment

Table 3
Ratio between the wall-clock time needed by the multilayer models with M layers ($t_{multi(M)}$) and the 3rd, 4th and 5th order moment models ($t_{moment(3rd)}, t_{moment(4th)}, t_{moment(5th)}$).

	$M=5$	$M=10$	$M=20$	$M=40$	$M=80$	$M=160$	$M=320$
$t_{multi(M)}/t_{moment(5th)}$	3.5	6.0	11.6	25.1	62.1	177.2	562.9
$t_{multi(M)}/t_{moment(4th)}$	4.5	7.8	15.1	32.8	81.2	231.5	735.3
$t_{multi(M)}/t_{moment(3rd)}$	5.7	9.8	19.1	41.3	102.2	291.3	925.4

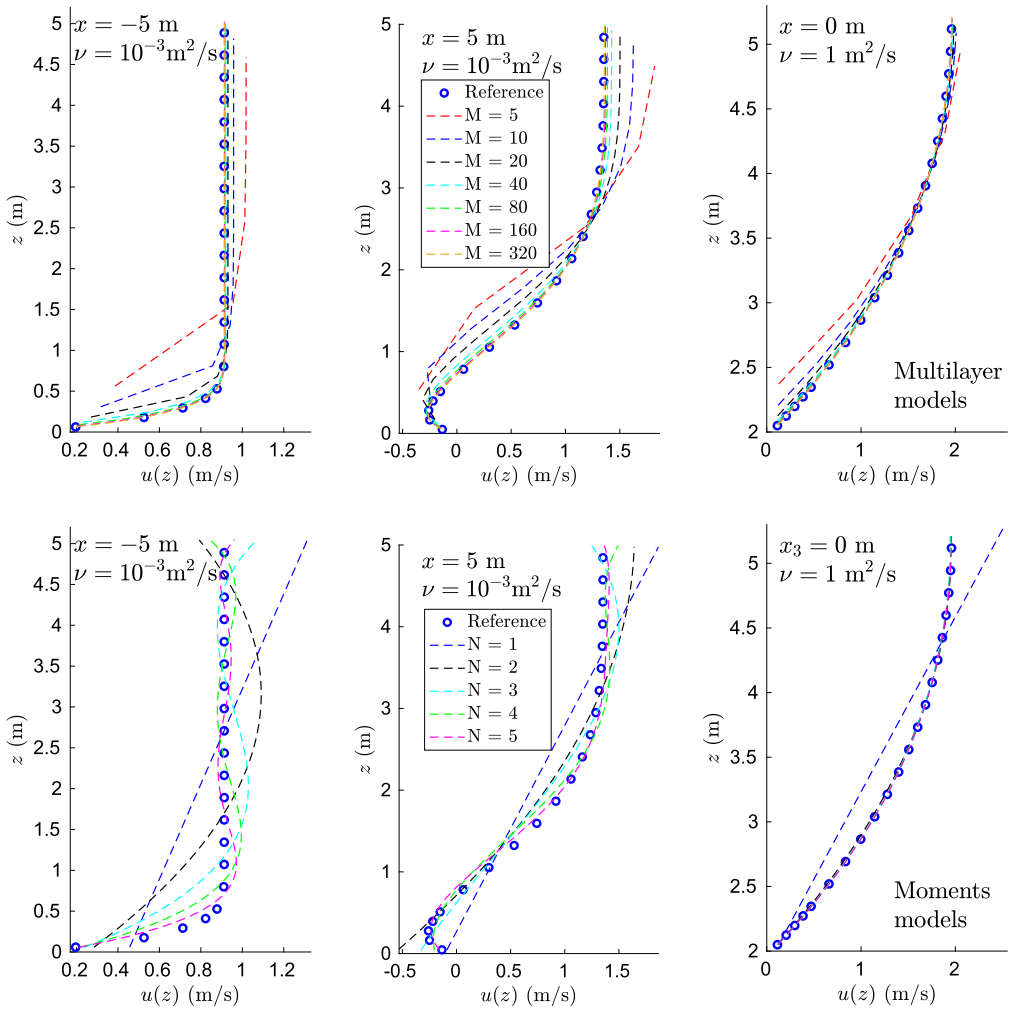

Fig. 5. Vertical profiles of velocity computed with the multilayer (upper figures) and moment (lower figures) models. Left hand side and center figures correspond to the low viscosity case whereas right hand side figures correspond to the high viscosity case.

model is 6 times faster when compared to the multilayer model with 10 layers and 25 times faster when using 40 vertical layers. This ratio increases to up to 62 if we double to 80 the number of layers.

In Fig. 4 we see the comparison of the wall-clock time with the L^2 relative errors on the velocity. We choose the error on the velocity field because it is the variable for which the errors are the largest. In the low viscosity case, we see that the 5th order moment model is comparable to the multilayer with 40 layers and better than the multilayer with 160 layers, in the sense that these errors are lower.

Let us now focus on the different profiles of velocity that we observe in these cases and how multilayer and moment models approximate them. We obtain three kinds of profiles depending on the magnitude of vertical effects. First, in the low viscosity case, we obtain a straight profile for a wide zone of the vertical domain (left-hand side plots in Fig. 5), and the velocity decreases close to the bottom because of the friction force. The low order moment models badly approximate this kind of profiles as it is difficult to fit them with a first or second order polynomial, due to the lack of sufficient vertical resolution. If we increase the order of the moment model, then we observe the oscillating intrinsic nature of polynomials. This fact is in particular observed for the fifth order moment model in the left bottom picture in Fig. 5. By increasing

Table 4
Relative errors made on the vertical profile of velocity for three different profiles: quasi-straight ($x = -5, \nu = 10^{-3}$ m^2/s), profile with recirculation ($x = 5, \nu = 10^{-3}$ m^2/s) and parabolic ($x = 0, \nu = 1$ m^2/s) profile. Results are shown for the multilayer (M layers) and the moment models (order N).

	$\mathrm{Err}_2^z\ [u,-5]$ ($\nu = 10^{-3}$)	$\mathrm{Err}_2^z\ [u,5]$ ($\nu = 10^{-3}$)	$\mathrm{Err}_2^z\ [u,0]$ ($\nu = 1$)	$\mathrm{Err}_\infty^z\ [u,-5]$ ($\nu = 10^{-3}$)	$\mathrm{Err}_\infty^z [u,5]$ ($\nu = 10^{-3}$)	$\mathrm{Err}_\infty^z\ [u,0]$ ($\nu = 1$)
M			Multilayer	(M layers)		
5	2.22×10^{-1}	3.51×10^{-1}	1.25×10^{-1}	4.40×10^{-1}	3.80×10^{-1}	1.83×10^{-1}
10	1.33×10^{-1}	2.25×10^{-1}	5.66×10^{-2}	3.83×10^{-1}	2.67×10^{-1}	9.40×10^{-2}
20	6.70×10^{-2}	1.29×10^{-1}	2.67×10^{-2}	2.61×10^{-1}	1.56×10^{-1}	4.72×10^{-2}
40	3.24×10^{-2}	6.33×10^{-2}	1.26×10^{-2}	1.60×10^{-1}	7.81×10^{-2}	2.31×10^{-2}
80	1.49×10^{-2}	2.94×10^{-2}	5.84×10^{-3}	8.69×10^{-2}	3.66×10^{-2}	1.08×10^{-2}
160	6.26×10^{-3}	1.27×10^{-2}	2.49×10^{-3}	4.02×10^{-2}	1.59×10^{-2}	4.65×10^{-3}
320	2.06×10^{-3}	4.28×10^{-3}	8.28×10^{-4}	1.39×10^{-2}	5.37×10^{-3}	1.55×10^{-3}
N			Moment	(order N)		
1	2.51×10^{-1}	2.31×10^{-1}	1.57×10^{-1}	4.39×10^{-1}	3.84×10^{-1}	2.77×10^{-1}
2	1.89×10^{-1}	1.48×10^{-1}	1.03×10^{-2}	4.06×10^{-1}	2.97×10^{-1}	1.34×10^{-2}
3	1.22×10^{-1}	9.66×10^{-2}	5.00×10^{-3}	3.15×10^{-1}	1.42×10^{-1}	5.98×10^{-3}
4	7.49×10^{-2}	6.95×10^{-2}	2.28×10^{-3}	2.14×10^{-1}	1.04×10^{-1}	2.69×10^{-3}
5	4.34×10^{-2}	4.79×10^{-2}	1.25×10^{-3}	1.27×10^{-1}	7.26×10^{-2}	1.50×10^{-3}

the order of the moment model N, the profiles are nearer to the reference solution. Nevertheless, the oscillations are still present. Secondly, we see a profile of velocity corresponding to recirculation of the flow (central plots in Fig. 5). These profiles are well reproduced by high order moment models ($N = 4, 5$), whereas low order models ($N < 4$) fail. Remark that the multilayer model needs more than 10 layers to reproduce this effect. Finally, we observe parabolic profiles (right hand side plots in Fig. 5). As expected, these profiles are efficiently and properly reproduced by moment models for order $N > 1$. We also see the convergence to the reference solution in all these profiles.

Table 4 shows the errors with respect the reference solution for these three profiles. We see that for the parabolic profile ($x = 0$), the moment model with $N > 1$ gives better results than multilayer models. The errors are larger for the other profiles ($x = -5$ or $x = 5$), but higher moments give good results, only comparable to using many layers in the multilayer case.

In conclusion, if the vertical profile of velocity is close to a polynomial, the moment approach allows us to obtain good results with less computational effort than the multilayer model, which needs many layers. However, if one needs to reproduce cases with large areas where a straight profile is found, the moment approach will oscillate due to its polynomial nature. That is eventually a limitation of the usual formulation of moment models. In this case, the multilayer model may be more appropriate, although a sufficiently large number of layers would still be needed.

4.2. Comparison of multilayer and moment models with Navier-Stokes

Let us now consider a numerical test included in [30] (Section 5.2) where a qualitative comparison with a Navier-Stokes solver in a simplified configuration is performed. Concretely, the test is described in [30] as follows. They carried out a simulation with the multilayer model, and the obtained stationary free surface is imposed as the fluid domain in the FreeFem++ solver [39] to solve the pressure and velocity fields. The authors checked that the simulation was in the hydrostatic framework, and they compared the obtained velocity profiles with both the multilayer method and FreeFem++. A reasonable agreement between the obtained profiles was found, where the differences are most undoubtedly due to how boundary conditions are imposed in the finite element solver and the multilayer model with a finite volume method.

To compare with the multilayer and moment models, we consider a fluid domain $[0, 3]$ discretized with 200 nodes and $CFL = 0.8$. In these simulations, a non-slip condition was used in the FreeFem++ code, so we consider here a large enough friction coefficient to reproduce this boundary condition. In practice, after a convergence analysis in ϵ, we use $\epsilon = 10^6$. For the viscosity, two values are considered, $\nu = 5\times10^{-4}$ and $\nu = 10^{-3}$ m^2/s.

We write here the initial and boundary conditions: the flow is initially at rest, and the initial bottom and free surface are given by

$$b_0(x) = \begin{cases} 0 & \text{if } x \le 1, \\ 0.5\,(x-1) & \text{if } 1 \le x \le 2, \\ 0.5 & \text{if } x \ge 2, \end{cases} \qquad b_0(x) + h_0(x) = 1 \text{ m} \qquad \text{at } t = 0 \text{ s},$$

and subcritical boundary conditions are imposed:

$$q(0,t) = \frac{2z}{h}\ \text{m}^2/\text{s} \quad \text{at } x = 0 \text{ m}; \qquad h(3,t) + b(3) = 1.2 \text{ m} \quad \text{at } x = 3 \text{ m}.$$

Fig. 6 shows the fluid domain with the stationary free surface, once it has been reached, where we focus on the velocity profiles at locations $x = 1.26$ and 1.74 m. We obtain the velocity profiles in these two points and compare them with the

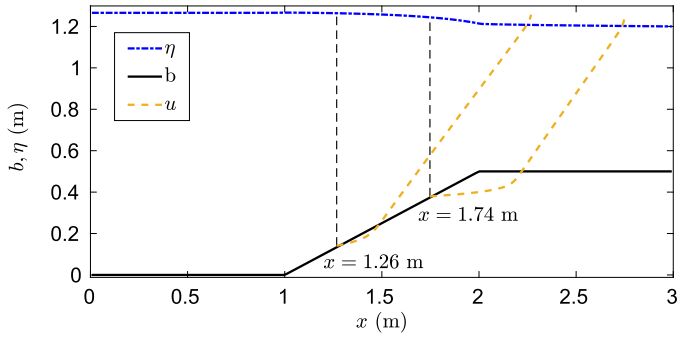

Fig. 6. Fluid domain with velocity profiles at $x = 1.26,\ 1.74$ m for the case $\nu = 10^{-3}$ m^2/s.

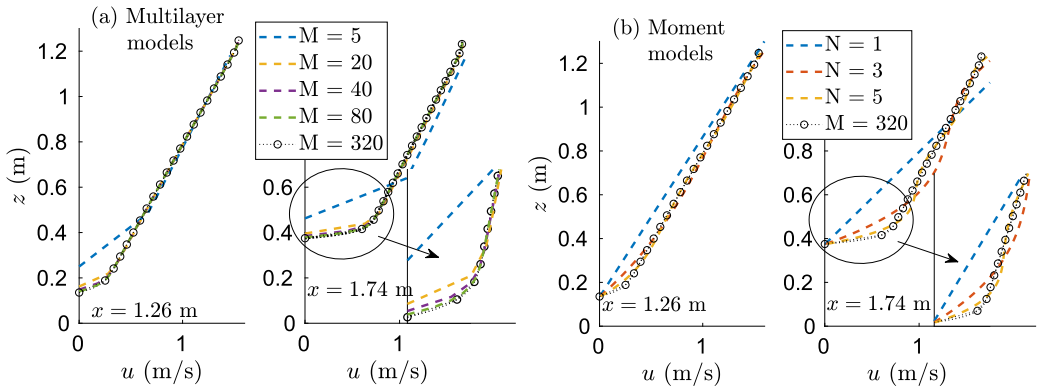

Fig. 7. Convergence of vertical profiles of velocity computed with the multilayer (left figures) and moment (right figures) models at locations $x = 1.26, 1.74$ m.

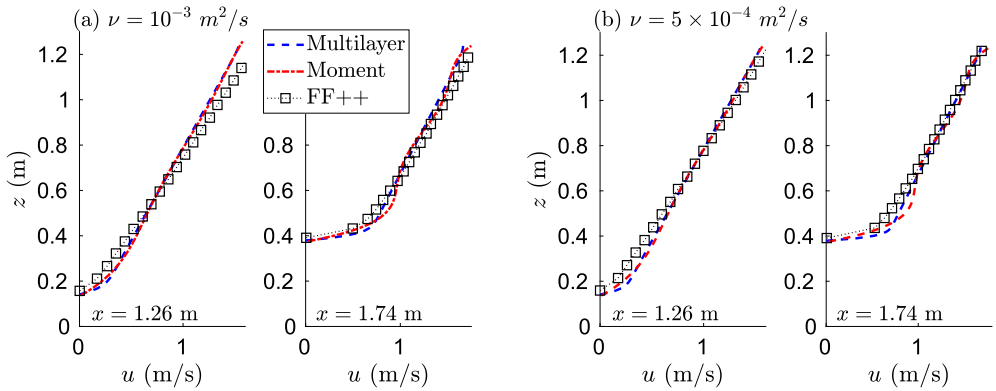

Fig. 8. Vertical profiles of velocity computed with the multilayer ($M = 80$) and moment ($N = 5$) models (lines) and the FreeFem++ solution (symbols) at locations $x = 1.26, 1.74$, for two values of the viscosity $\nu = 10^{-3}$ (left figures) and $\nu = 5 \times 10^{-4}$ m^2/s (right figures).

corresponding finite element solution. First, we show the convergence of the velocity profiles for both the multilayer and moment approach to a reference solution computed with a large number of layers (see Fig. 7), in the case $\nu = 10^{-3}$. We see that the velocity profiles in these points exhibit a parabolic shape near the bottom due to the friction force, and then they become a linear profile. As expected, both approaches reproduce well these profiles, although we see the oscillatory character of the moment approach, especially in the straight part of the vertical profile. The same behavior is observed when comparing with the FreeFem++ solutions for $\nu = 10^{-3}, 5 \times 10^{-4}$ m^2/s (see Fig. 8). We see that the obtained profiles are in good agreement with the finite volume solution, in concordance with [30]. Similarly to what was said in that work, we conclude that the observed differences are most surely due to the way of imposing boundary conditions in both solvers, and also the rest of the characteristics of both solvers (mainly, non-hydrostatic pressure and stationary with the fixed free surface approach of the performed FreeFem++ simulation in [30]).

4.3. Numerical convergence for stationary analytical solutions of the free-surface hydrostatic Euler equations

We focus now on comparing the usual multilayer model (19) and the one introduced here with a layerwise linear velocity (21). We consider two discretizations for the velocity at the vertical interfaces (see Appendix A), a centered (C) definition

$$\widetilde{u}_{\alpha+1/2} = \frac{u^{+}_{\alpha+1/2} + u^{-}_{\alpha+1/2}}{2},$$

and an upwind (U) definition

$$\widetilde{u}_{\alpha+1/2} = \frac{u^{+}_{\alpha+1/2} + u^{-}_{\alpha+1/2}}{2} - \frac{sign\left(-\omega_{\alpha+1/2}\right)}{2}\left(u^{+}_{\alpha+1/2} - u^{-}_{\alpha+1/2}\right).$$

From now on, we shall denote by MCC and MCU the Multilayer Constant Central and the Multilayer Constant Upwind models, that is, the usual multilayer models with either a central or upwind definition of the velocity at the interface. Similarly, MLC and MLU will stand for Multilayer Linear Central and Multilayer Linear Upwind models with layerwise linear velocities.

We consider a set of continuous stationary solutions for the hydrostatic Euler system (6) derived in [10]. More precisely, we consider the general continuous stationary solution given by

$$\begin{cases} z_b(x) = \bar{z}_b - h(x) - \dfrac{\alpha^2\beta^2}{2g\sin^2(\beta h(x))}, \\ \widetilde{u}(x,\xi) = \dfrac{\alpha\beta}{\sin(\beta h(x))}\cos(\xi\beta h(x)), \end{cases} \tag{22}$$

where α, β and $\bar{z}_b$ are three real constants, and $h(x)$ is a non-negative continuous function such that $\sin(\beta h(x)) \neq 0$ for all x in the horizontal fluid domain.

This test problem aims to inspect the abilities of the proposed vertical discretizations to preserve stationary solutions of the free-surface hydrostatic Euler equations and numerically state the expected order of accuracy.

To do that we consider

$$x \in [-5,\ 5], \quad \alpha = \beta = -1, \quad \bar{z}_b = 0,$$

and

$$h(x) = 1.4 - 0.8e^{-x^2}, \tag{23}$$

for the total water depth (see Fig. 9). Once the height is fixed, the bottom is given by (22). Then, given a vertical discretization into M layers, we consider as initial condition for the horizontal velocity

$$u_\alpha(x,\xi) = \widehat{u}_{\alpha,0}(x)\widehat{\phi}_{\alpha,0}(\xi) + \widehat{u}_{\alpha,1}(x)\widehat{\phi}_{\alpha,1}(\xi), \quad \alpha \in \{1,\dots,M\},$$

the piecewise linear projection of the function $\widetilde{u}$ in (22) as given in (8), i.e.,

$$\widehat{u}_{\alpha,j}(x) = \frac{1}{l_\alpha \mu_j}\int_{L_{\alpha-1/2}}^{L_{\alpha+1/2}} \widetilde{u}(x,\xi)\hat{\phi}_{\alpha,j}(\xi)\,d\xi, \quad \text{for } j = 0,1 \text{ and } \alpha \in \{1,\dots,M\}. \tag{24}$$

We then compute different numerical approximations for a final time $t = 10$ s with a set of refined meshes and other values of the number of layers M. Dirichlet boundary conditions have been used by imposing the values of the stationary solution at both ends of the domain. We consider in this case the L^1 absolute errors. Such errors are computed against the initial condition, that coincides with the L^1 projection of the exact solution into the space of linear polynomials in ξ. More precisely, we consider in this case the errors given by

$$\|h - h^{ref}\|_1 = \Delta x \sum_{i=1}^{N_x}\left|h_i - \widetilde{h}_i^{ref}\right|, \quad \|u - u^{ref}\|_1 = \Delta x \sum_{i,\alpha=1}^{N_x,M}\int_{L_{\alpha-1/2}}^{L_{\alpha+1/2}}\left|u_{\alpha,i}(\xi) - \widetilde{u}_{\alpha,i}^{ref}(\xi)\right|d\xi, \tag{25}$$

where the last integral will be computed by using the Simpson's rule. As it is said above, in this test the reference solution is given by the initial state.

Table 5 shows the L^1 errors and the numerical convergence rates. It is essential to make some remarks. First, note that a usual formal order analysis has been performed, where $\Delta x \approx \Delta z$, and an increasing number of cells has been considered for

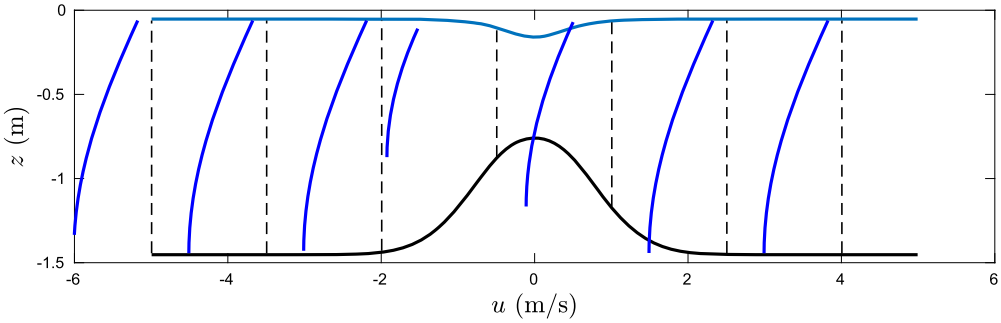

Fig. 9. Initial free-surface and vertical profiles of velocity u at locations $x = -5,\ -3.5,\ -2,\ -0.5,\ 1,\ 2.5$, and 4 m. for the stationary solution given by (23)-(24).

Table 5
Numerical convergence results for the initial condition (23)-(24). The L^1 errors refer to the variables h and u at a final time $t = 10$ s, measured for different vertical discretizations of M layers and using uniform Cartesian meshes of N_x elements.

M	N_x	$\|h - h^{ref}\|_1$	Order$_h$	$\|u - u^{ref}\|_1$	Order$_u$	$\|h - h^{ref}\|_1$	Order$_h$	$\|u - u^{ref}\|_1$	Order$_u$
		MCU				MCC			
10	100	7.24×10^{-3}	-	1.76×10^{-1}	-	6.51×10^{-3}	-	5.19×10^{-2}	-
20	200	4.54×10^{-3}	0.67	1.07×10^{-1}	0.72	1.63×10^{-3}	2.00	1.42×10^{-2}	1.87
40	400	2.78×10^{-3}	0.71	5.90×10^{-2}	0.86	3.99×10^{-4}	2.03	3.50×10^{-3}	2.02
80	800	1.54×10^{-3}	0.86	3.10×10^{-2}	0.93	9.81×10^{-5}	2.02	8.36×10^{-4}	2.07
		MLU				MLC			
10	100	6.56×10^{-3}	-	5.15×10^{-2}	-	6.58×10^{-3}	-	5.22×10^{-2}	-
20	200	1.64×10^{-3}	2.00	1.43×10^{-2}	1.85	1.65×10^{-3}	2.00	1.45×10^{-2}	1.85
40	400	4.00×10^{-4}	2.03	3.42×10^{-3}	2.06	3.98×10^{-4}	2.05	3.42×10^{-3}	2.08
80	800	9.77×10^{-5}	2.03	8.31×10^{-4}	2.04	9.80×10^{-5}	2.02	8.32×10^{-4}	2.04

computing the expected order of accuracy of the vertical and horizontal numerical approximation methods of free-surface Euler equations. Note that the desired order of accuracy is achieved for the MLU and MLC methods since they provide second order of accuracy in the vertical direction. Concerning the MC methods, note that MCC provides a second order of accuracy on the vertical, whereas the MCU is expected to provide first order of accuracy. Finally, note the efficiency of ML methods over MC. To get a L^1 error equal or less to 1×10^{-2} for the velocity u, the MCU and MCC need more than $M = 80$ and $M = 20$ layers, respectively, whereas the MLU and MLC approximation reach errors less than 1×10^{-2} with less than $M = 30$ and $M = 20$ layers. A deeper analysis of the efficiency, including elapsed times, will be done in the following subsection.

4.4. Perturbed stationary analytical solutions for the free-surface hydrostatic Euler equations

We consider now a perturbation of the stationary solution (22)-(23). We take the same initial conditions except for the velocity, for which we assume

$$\widetilde{u}(x, \xi) = \frac{\alpha\beta}{\sin(\beta\,(h(x) - 0.1))} \cos(\xi\beta\,(h(x) - 0.1)). \tag{26}$$

The computational domain is now $[-10, 10]$, and the parameters are set to $\alpha = \beta = -1$, and $\bar{z}_b = 0$, as previously. In this case, periodic boundary conditions are imposed. We then compute different numerical approximations until a final time $t = 1$ s with a set of refined meshes in the vertical direction with different values of the number of layers M.

Table 6 shows the L^1 errors and the numerical convergence rates. Errors are computed as in (25), but considering a reference solution that has been computed with the Multilayer Constant Central method with $N_x = 1600$ elements and $M = 160$ layers. As it can be seen, the proposed methods provide an accurate approximation as expected, and similar conclusions as in the previous test case may be reached. It is important to emphasize the outstanding performance of ML methods compared to MC ones.

Table 7 shows the computational time needed by both models for several layers, as well as its ratio. In terms of the computational effort, the model MLU is approximately 1.5 times more expensive than the MCU for a given number of layers M. That is natural since M extra equations, corresponding to $\widehat{u}_{\alpha,1}$, are solved in the layerwise linear velocity case. However, the gain of the accuracy is worth it by far. It can be concluded from the Tables 5 and 6, and also from Fig. 10, where we show the computational times against the error made on the velocity field, for the cases $M = 5, 10, 20, 40$ layers. In particular, we see that the MLU model with $M = 5$ layers improves the results of the MCU model with $M = 40$ layers, with a lower computational effort.

Table 6
Numerical convergence results for the initial condition (26). The L^1 errors refer to the variable u at a final time $t = 1$ s, measured for different vertical discretizations of N layers and using uniform Cartesian meshes of $N_x = 1600$ elements.

M	N_x	$\|u - u^{ref}\|_1$	Order_u	$\|u - u^{ref}\|_1$	Order_u	$\|u - u^{ref}\|_1$	Order_u	$\|u - u^{ref}\|_1$	Order_u
		MCU		MCC		MLU		MLC	
5	1600	3.42×10^{-2}	-	9.03×10^{-3}	-	7.91×10^{-4}	-	1.47×10^{-3}	-
10	1600	1.71×10^{-2}	1.00	2.29×10^{-3}	1.98	1.44×10^{-4}	2.46	3.69×10^{-4}	1.99
20	1600	8.63×10^{-3}	0.98	5.72×10^{-4}	2.00	2.56×10^{-5}	2.49	9.38×10^{-5}	1.98
40	1600	4.33×10^{-3}	0.99	1.41×10^{-4}	2.01	5.84×10^{-6}	2.13	2.49×10^{-5}	1.91

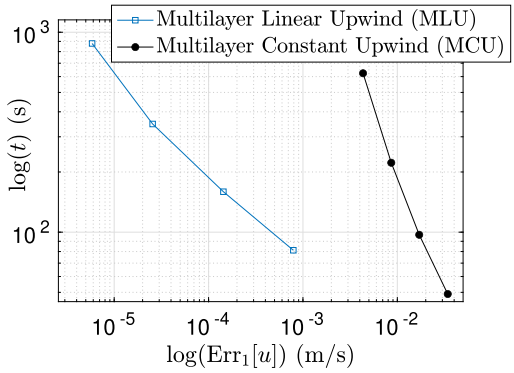

Fig. 10. Computational time and errors on the velocity field, in log scale, for the MCU (black circles) and MLU (blue squares) models at $t_f = 10$ s, with $M = 5, 10, 20, 40$ layers and $N_x = 1600$ cells.

Table 7
Wall clock times of MCU ($t_{\text{MCU(M)}}$) and MLU ($t_{\text{MLU(M)}}$) models to reach $t_f = 10$ s, and ratios, with $M = 5, 10, 20, 40$ layers and $N_x = 1600$ cells.

	$M = 5$	$M = 10$	$M = 20$	$M = 40$
$t_{\text{MCU(M)}}$ (s)	49.1	97.1	222.6	623.9
$t_{\text{MLU(M)}}$ (s)	81.1	159.3	347.6	878.7
$t_{\text{MLU(M)}}/t_{\text{MCU(M)}}$	1.65	1.64	1.56	1.41

5. Conclusions

A general framework for vertical discretizations of Euler equations has been proposed. It is based on considering a change to σ-coordinates and a partition on M layers along the vertical direction of the interval $[0, 1]$. Then a polynomial approximation of the variables, with arbitrary degree N, is assumed. The derivation procedure performed is general enough to extend it to other cases (e.g. non-hydrostatic pressure regimes, passive scalar transport, among many others). This model may be seen as a semi-discrete vertical discretization of the Euler system written in σ-coordinates in the framework of the Discontinuous Galerkin methods.

As particular cases of the discretization introduced here, we immediately recover, as simplified configurations, the usual multilayer and moment models appearing in the literature. Therefore, both can be seen as particular vertical discretizations under the same framework. In addition, an enriched multilayer-moment model has been proposed, particularly a multilayer model with a layerwise linear horizontal velocity.

In the numerical test cases, we have shown comparisons of usual moment a multilayer approaches, pointing out some advantages/limitations of both methods. We have shown that, in general, high order moment models allow us to recover the solution of multilayer models with a much smaller computational effort, so then they are much more efficient. It is especially relevant when the velocity field exhibits a parabolic profile along the whole domain. However, multilayer models may be more appropriate when the velocity profile has straight zones since moment models introduce oscillations due to the polynomial approximation. Finally, we have shown that the multilayer model with layerwise linear velocity proposed here preserves a fully 2D steady solution of hydrostatic Euler equations, different from water at rest, up to second order accuracy. Moreover, when introducing a perturbed initial condition, we recover the desired order of accuracy of both approaches: multilayer model with layerwise constant velocity is first order accurate. In contrast, second order is obtained with the proposed model considering a layerwise linear velocity. We have also measured the efficiency of the MLU model for the MCU model. Despite being 1.5 times more expensive in terms of computational efforts for a fixed number of layers, we have shown that it makes sense to use it in terms of accuracy. Actually, with the proposed layerwise linear velocity model, we need just a few layers to improve the results of the usual multilayer model with a high number of vertical layers. In the future, it would be interesting to extend the proposed model to the non-hydrostatic case, as well as studying

local strategies to adapt a variable number of the vertical layers and/or a variable polynomial degree for efficiency purposes, following the ideas in [1,31].

Acknowledgements

This research has been partially supported by the Spanish Government and FEDER through the research projects RTI2018-096064-B-C2(1/2) and PID2020-114688RB-I00, the Junta de Andalucía research project P18-RT-3163, the Junta de Andalucia-FEDER-University of Málaga research project UMA18-FEDERJA-16. Funding for open access charge: Universidad de Málaga / CBUA.

Appendix A. Viscous multilayer-moment systems and continuity conditions at the interfaces

This appendix is devoted to describe, for the sake of completeness, how the viscous terms are included in the derivation of the models. Although this work focuses mainly in Euler equation, they are relevant for some of the simulations and they allow to properly define the velocities at the interfaces $u_{|_{L^{\pm}_{\alpha+1/2}}}$.

We first detail the general procedure and then describe the viscous system in the particular case of layerwise constant velocities (Multilayer Constant method).

A.1. Multilayer-moment system

Let us first recall that for any variable $f \equiv f(t,x,\xi)$, we shall denote by $f^{\pm}_{\alpha+1/2} = f_{|_{\xi=L^{\pm}_{\alpha+1/2}}}$ the upper or lower limit at the interface $L_{\alpha+1/2}$. When the variable is continuous at the interface, we simply denote it by $f_{\alpha+1/2}$. We shall denote by

$$[f]_{\alpha+1/2} = f^{+}_{\alpha+1/2} - f^{-}_{\alpha+1/2}.$$

Let us focus on (2a) in the hydrostatic case, but keeping now the viscous terms:

$$\begin{cases} \partial_t h + \partial_x(hu) - \partial_\xi \omega = 0, \\ \partial_t (hu) + \partial_x \left(hu^2\right) + gh\partial_x \eta = \partial_x(h\tau_{xx}) + \partial_\xi \left(\omega u + \tau_{xz} - \tau_{xx}\partial_x(h\xi + b)\right), \\ \omega = \partial_x \left(h \left(\int_0^\xi u_{|_{\xi=s}} ds - \xi \overline{u} \right) \right). \end{cases}$$

Recall that, from the definition of ω, we get $\omega^{+}_{\alpha+1/2} = \omega^{-}_{\alpha+1/2}$. Then, integrating the second equation for $s \in [0,\xi]$ we have

$$\begin{aligned} &(u\omega + \tau_{xz} - \partial_x(h\xi + b)\tau_{xx})_{|_\xi} - \left((\tau_{xz})_{|_{\xi=0}} - \partial_x(b)(\tau_{xx})_{|_\xi}\right) \\ &\qquad = \partial_t \left(h \int_0^\xi u(s)ds \right) + \partial_x \left(h \int_0^\xi (u^2 - \tau_{xx})(s) \right) ds + gh\xi\partial_x\eta \end{aligned}$$

Notice that in particular this means that $(u\omega + \tau_{xz} - \partial_x(h\xi + b)\tau_{xx})$ is continuous at the interfaces $L_{\alpha+1/2}$. In particular,

$$[u\omega + \tau_{xz} - \partial_x(h\xi + b)\tau_{xx}]_{\alpha+1/2} = 0,$$

or equivalently

$$[-\tau_{xz} + \partial_x(h\xi + b)\tau_{xx}]_{\alpha+1/2} = [u]_{\alpha+1/2}\, \omega_{\alpha+1/2}. \tag{A.1}$$

Remark 7. Using a similar framework as the one introduced in [30], continuity of ω and $u\omega + \tau_{xz} - \partial_x(h\xi + b)\tau_{xx}$ at the interfaces may be interpreted as the jump conditions for the mass and the horizontal momentum conservation equations verified by a weak solution of the Navier-Stokes system.

Denote by $\sigma = -\tau_{xz} + \partial_x(h\xi + b)\tau_{xx}$ and remark that

$$\int_{L_{\alpha-1/2}}^{L_{\alpha+1/2}} \partial_\xi(\omega u - \sigma)d\xi = \omega_{\alpha+1/2}u^{-}_{\alpha+1/2} - \sigma^{-}_{\alpha+1/2} - \omega_{\alpha-1/2}u^{+}_{\alpha-1/2} + \sigma^{+}_{\alpha-1/2},$$

where $\sigma^{-}_{\alpha+1/2}, \sigma^{+}_{\alpha-1/2}$ should be correctly defined.

In [30], this is done by means of a centered approximation $\widetilde{\sigma}_{\alpha+1/2}$ at the interface:

$$\widetilde{\sigma}_{\alpha+1/2} = \frac{\sigma^+_{\alpha+1/2} + \sigma^-_{\alpha+1/2}}{2}.$$

Nevertheless, one could do other possible choices as we will see.

In general, a given approximation at the interfaces may be done by considering a vertical numerical flux $\mathcal{G}$ depending on the upper and lower limit values at the interface. For the sake of generality, let us consider

$$\widetilde{\sigma}_{\alpha+1/2} = \mathcal{G}\left(\sigma^-_{\alpha+1/2}, \sigma^+_{\alpha+1/2}\right) = \frac{\sigma^+_{\alpha+1/2} + \sigma^-_{\alpha+1/2}}{2} - \frac{\Lambda_{\alpha+1/2}}{2}\left(\sigma^+_{\alpha+1/2} - \sigma^-_{\alpha+1/2}\right), \tag{A.2}$$

where the term $\Lambda_{\alpha+1/2}$ allows us to include an upwind term on the definition of $\widetilde{\sigma}_{\alpha+1/2}$.

By writing

$$\sigma^-_{\alpha+1/2} = \left(\frac{\sigma^+_{\alpha+1/2} + \sigma^-_{\alpha+1/2}}{2}\right) - \left(\frac{\sigma^+_{\alpha+1/2} - \sigma^-_{\alpha+1/2}}{2}\right),$$

then we have

$$\begin{aligned}\sigma^-_{\alpha+1/2} &= \left(\widetilde{\sigma}_{\alpha+1/2} + \frac{\Lambda_{\alpha+1/2}}{2}\left(\sigma^+_{\alpha+1/2} - \sigma^-_{\alpha+1/2}\right)\right) - \left(\frac{\sigma^+_{\alpha+1/2} - \sigma^-_{\alpha+1/2}}{2}\right)\\ &= \widetilde{\sigma}_{\alpha+1/2} - \frac{1}{2}(1-\Lambda_{\alpha+1/2})\,[\sigma]_{\alpha+1/2} = \widetilde{\sigma}_{\alpha+1/2} - \frac{1}{2}(1-\Lambda_{\alpha+1/2})\,[u]_{\alpha+1/2}\,\omega_{\alpha+1/2},\end{aligned}$$

where (A.1) has been used. Therefore,

$$\begin{aligned}\omega_{\alpha+1/2}u^-_{\alpha+1/2} - \sigma^-_{\alpha+1/2} - &= \omega_{\alpha+1/2}u^-_{\alpha+1/2} - \widetilde{\sigma}_{\alpha+1/2} + \frac{1}{2}(1-\Lambda_{\alpha+1/2})[u]_{\alpha+1/2}\omega_{\alpha+1/2}\\ &= \omega_{\alpha+1/2}\widetilde{u}_{\alpha+1/2} - \widetilde{\sigma}_{\alpha+1/2},\end{aligned}$$

where

$$\widetilde{u}_{\alpha+1/2} = \mathcal{G}\left(u^-_{\alpha+1/2}, u^+_{\alpha+1/2}\right) = \frac{u^+_{\alpha+1/2} + u^-_{\alpha+1/2}}{2} - \frac{\Lambda_{\alpha+1/2}}{2}\left(u^+_{\alpha+1/2} - u^-_{\alpha+1/2}\right). \tag{A.3}$$

In a similar way one obtains

$$\begin{aligned}\sigma^+_{\alpha-1/2} &= \left(\widetilde{\sigma}_{\alpha-1/2} + \frac{\Lambda_{\alpha-1/2}}{2}\left(\sigma^+_{\alpha-1/2} - \sigma^-_{\alpha-1/2}\right)\right) + \left(\frac{\sigma^+_{\alpha-1/2} - \sigma^-_{\alpha-1/2}}{2}\right)\\ &= \widetilde{\sigma}_{\alpha-1/2} + \frac{1}{2}(1+\Lambda_{\alpha-1/2})\,[\sigma]_{\alpha-1/2} = \widetilde{\sigma}_{\alpha-1/2} + \frac{1}{2}(1+\Lambda_{\alpha-1/2})\,[u]_{\alpha-1/2}\,\omega_{\alpha-1/2},\end{aligned}$$

and

$$\omega_{\alpha-1/2}u^+_{\alpha-1/2} - \sigma^+_{\alpha-1/2} = \omega_{\alpha-1/2}\widetilde{u}_{\alpha-1/2} - \widetilde{\sigma}_{\alpha-1/2},$$

which leads us to

$$u^-_{\alpha+1/2}\omega_{\alpha+1/2} - u^+_{\alpha-1/2}\omega_{\alpha-1/2} - \widetilde{\sigma}^-_{\alpha+1/2} + \widetilde{\sigma}^+_{\alpha-1/2} = \widetilde{u}_{\alpha+1/2}\,\omega_{\alpha+1/2} - \widetilde{u}_{\alpha-1/2}\,\omega_{\alpha-1/2} - \widetilde{\sigma}_{\alpha+1/2} + \widetilde{\sigma}_{\alpha-1/2}. \tag{A.4}$$

Finally, (18) is recovered from (A.4) when going to the limit of ν tending to zero to recover Euler equations.

Remark 8. There is a compatibility condition between definitions (A.2) and (A.3) for $\widetilde{\tau}$ and $\widetilde{u}$, in the sense that the numerical flux we consider to define $\widetilde{\tau}_{\alpha+1/2}$, in view of (A.1), is the flux we recover for the definition of the velocity at the interface $\widetilde{u}_{\alpha+1/2}$.

For instance, in [30,27,32,8] a central flux ($\Lambda = 0$) is considered, whereas an upwind numerical flux ($\Lambda = sign\,(-\omega)$) is taken in [6,5,36,31], mainly for stability reasons, where the sign of $-\omega$ matches with the sign of the vertical velocity (see (2b)).

Nevertheless, (A.2) and (A.3) correspond formally to the consistency with the viscous terms. In the general case this could be not sufficient to grant stability and, in particular, for $M > 1$ and $N > 0$ appropriate penalization terms would be needed to make sure that the discretization converges as shown in [20,2].

A.2. Viscous multilayer constant method

We consider now the viscous Multilayer Constant (MC) case, where we recall that the velocity is layerwise constant. With the goal of keeping the friction force and vertical viscosity effects, we consider the leading order approximation

$$\widetilde{\sigma} = -\widetilde{\tau_{xz}} = -\frac{\nu}{h}\,\widetilde{\partial_\xi u},$$

which is easily justified from an asymptotic analysis. Then, from (A.4) we get

$$\frac{\nu}{h}\left(\widetilde{\partial_\xi u}\right)_{\alpha+1/2} - \frac{\nu}{h}\left(\widetilde{\partial_\xi u}\right)_{\alpha-1/2} + \widetilde{u}_{\alpha+1/2}\,\omega_{\alpha+1/2} - \widetilde{u}_{\alpha-1/2}\,\omega_{\alpha-1/2},$$

for a constant kinematic viscosity ν. By simplicity, consider here $\Lambda_{\alpha+1/2} = 0$ in (A.2), and therefore

$$\tau^{+}_{xz,\alpha+1/2} = \tau^{-}_{xz,\alpha+1/2} = \widetilde{\tau}_{xz,\alpha+1/2}.$$

In particular, we need to approximate $\left(\widetilde{\partial_\xi u}\right)_{\alpha+1/2}$. Concretely, we choose

$$\widetilde{\tau}_{xz,\alpha+1/2} = -\frac{\nu}{h}\,\left(\widetilde{\partial_\xi u}\right)_{\alpha+1/2} = -\frac{\nu}{h}\,\frac{u_{\alpha+1}-u_\alpha}{\frac{1}{2}\left(l_\alpha + l_{\alpha+1}\right)}.$$

Therefore, the viscous version of system (19), accounting for boundary conditions (2c), reads

$$\begin{cases} \partial_t h + \partial_x\left(h\overline{u}\right) = 0, \\ l_\alpha\left(\partial_t\left(hu_\alpha\right) + \partial_x\left(hu_\alpha^2\right) + gh\partial_x\left(b+h\right)\right) = K_{\alpha+1/2} - K_{\alpha-1/2} \\ \qquad + \dfrac{u_{\alpha+1}+u_\alpha}{2}\omega_{\alpha+1/2} - \dfrac{u_\alpha + u_{\alpha+1}}{2}\omega_{\alpha-1/2}, \qquad \text{for } \alpha = 1,\dots,M \end{cases} \tag{A.5a}$$

with

$$K_{\alpha+1/2} = \frac{\nu}{h}\frac{u_{\alpha+1}-u_\alpha}{\frac{1}{2}(l_{\alpha+1}+l_\alpha)}, \qquad \text{for } \alpha = 1,\dots,M-1, \tag{A.5b}$$

and the boundary conditions (2c) for the stress tensor $K_{M+1/2} = 0$, $K_{1/2} = \epsilon\,|u_1|\,u_1$. Finally, we have

$$\omega_{\alpha+1/2} = \sum_{\beta=1}^{\alpha} l_\beta \partial_x\left(h\left(u_\beta - \overline{u}\right)\right), \qquad \text{with} \qquad \overline{u} = \sum_{\beta=1}^{M} l_\beta u_\beta. \tag{A.5c}$$

Appendix B. Viscous shallow water moment model

Including the contribution of the viscous term $\partial_\xi \tau_{xz}$ in moment model (20) is a simple task. Proceeding as in [33], we compute the following integral for $i = 0,\dots,N$ (see (2a)) taking into account the boundary conditions (2c):

$$\begin{aligned} \int_0^1 \partial_\xi\left(\frac{\nu}{h}\partial_\xi u\right)\phi_i\,d\xi &= \frac{\nu}{h}\left(\partial_\xi u\right)_{|\xi=1}\phi_i(1) - \frac{\nu}{h}\left(\partial_\xi u\right)_{|\xi=0} - \sum_{j=0}^{N}\widehat{u}_j\int_0^1 \phi_i'\phi_j'\,d\xi \\ &= -\epsilon|u_{|\xi=0}|u_{|\xi=0} - \frac{\nu}{h}\sum_{j=1}^{N}\widehat{u}_j D_{ij}, \end{aligned}$$

where $D_{ij} = \int_0^1 \phi_i'\phi_j'\,d\xi$. Note that $D_{ij} = D_{ji}$, $D_{0j} = 0$, and $u_b := u_{|\xi=0} = \sum_{j=0}\widehat{u}_j$. Thus, the moment model with vertical viscosity reads

$$\begin{cases} \partial_t h + \partial_x (h\widehat{u}_0) = 0, \\ \partial_t (h\widehat{u}_0) + \partial_x \left(h\widehat{u}_0^2 + h \sum_{j=1}^{N} \frac{\widehat{u}_j^2}{2j+1} \right) + gh\, \partial_x \eta = -\epsilon |u_b| u_b, \\ \partial_t (h\widehat{u}_i) + \partial_x \left(2h\widehat{u}_0\widehat{u}_i + h\frac{1}{\mu_i} \sum_{j,k=1}^{N} A_{ijk}\widehat{u}_j\widehat{u}_k \right) = \widehat{u}_0 \partial_x (h\widehat{u}_i) - \frac{1}{\mu_i} \sum_{j,k=1}^{N} B_{ijk}\widehat{u}_k \partial_x (h\widehat{u}_j) \\ \qquad -\frac{1}{\mu_i} \left(\epsilon |u_b| u_b + \frac{\nu}{h} \sum_{j=1}^{N} \widehat{u}_j D_{ij} \right), \qquad \text{for } i = 1, \dots, N. \end{cases} \tag{B.1}$$

References

[1] A. Abbà, M. Tugnoli, L. Bonaventura, Dynamical p-adaptivity for LES of compressible flows in a high order DG framework, J. Comput. Phys. 420 (Nov. 2020) 109720.
[2] D.N. Arnold, F. Brezzi, B. Cockburn, L.D. Marini, Unified analysis of discontinuous Galerkin methods for elliptic problems, SIAM J. Numer. Anal. 39 (5) (Jan. 2002) 1749–1779.
[3] E. Audusse, A multilayer Saint-Venant model: derivation and numerical validation, Discrete Contin. Dyn. Syst., Ser. B 5 (2) (Feb. 2005) 189–214.
[4] E. Audusse, F. Bouchut, M. Bristeau, R. Klein, B. Perthame, A fast and stable well-balanced scheme with hydrostatic reconstruction for shallow water flows, SIAM J. Sci. Comput. 25 (6) (Jan. 2004) 2050–2065.
[5] E. Audusse, M.-O. Bristeau, M. Pelanti, J. Sainte-Marie, Approximation of the hydrostatic Navier-Stokes system for density stratified flows by a multilayer model: kinetic interpretation and numerical solution, J. Comput. Phys. 230 (9) (May 2011) 3453–3478.
[6] E. Audusse, M.-O. Bristeau, B. Perthame, J. Sainte-Marie, A multilayer Saint-Venant system with mass exchanges for shallow water flows derivation and numerical validation, ESAIM: Math. Model. Numer. Anal. 45 (1) (Jun. 2010) 169–200.
[7] C. Bassi, L. Bonaventura, S. Busto, M. Dumbser, A hyperbolic reformulation of the Serre-Green-Naghdi model for general bottom topographies, Comput. Fluids 212 (Nov. 2020) 104716.
[8] L. Bonaventura, E.D. Fernández-Nieto, J. Garres-Díaz, G. Narbona-Reina, Multilayer shallow water models with locally variable number of layers and semi-implicit time discretization, J. Comput. Phys. 364 (2018) 209–234.
[9] F. Bouchut, M. Westdickenberg, Gravity driven shallow water models for arbitrary topography, Commun. Math. Sci. 2 (3) (2004) 359–389.
[10] A.C. Boulanger, M.O. Bristeau, J. Sainte-Marie, Analytical solutions for the free surface hydrostatic Euler equations, Commun. Math. Sci. 11 (4) (2013) 993–1010.
[11] M.-O. Bristeau, C. Guichard, B. di Martino, J. Sainte-Marie, Layer-averaged Euler and Navier-Stokes equations, Commun. Math. Sci. 15 (5) (2017) 1221–1246.
[12] F.N. Cantero-Chinchilla, O. Castro-Orgaz, A.A. Khan, Vertically-averaged and moment equations for flow and sediment transport, Adv. Water Resour. 132 (Oct. 2019) 103387.
[13] M.J. Castro, A.M. Ferreiro Ferreiro, J.A. García-Rodríguez, J.M. González-Vida, J. Macías, C. Parés, M.E. Vázquez-Cendón, The numerical treatment of wet/dry fronts in shallow flows: application to one-layer and two-layer systems, Math. Comput. Model. 42 (3) (2005) 419–439.
[14] M.J. Castro, T. Morales de Luna, C. Parés, Well-balanced schemes and path-conservative numerical methods, in: Rémi Abgrall, Chi-Wang Shu (Eds.), Handbook of Numerical Analysis, in: Handbook of Numerical Methods for Hyperbolic Problems Applied and Modern Issues, vol. 18, Elsevier, 2017, pp. 131–175.
[15] M.J. Castro Díaz, E.D. Fernández-Nieto, A class of computationally fast first order finite volume solvers: PVM methods, SIAM J. Sci. Comput. 34 (4) (Jan. 2012) A2173–A2196.
[16] V. Casulli, A semi-implicit finite difference method for non-hydrostatic free-surface flows, Int. J. Numer. Methods Fluids 30 (4) (Jun. 1999) 425–440.
[17] V. Casulli, G.S. Stelling, Numerical simulation of 3D quasi-hydrostatic, free-surface flows, J. Hydraul. Eng. 124 (7) (Jul. 1998) 678–686.
[18] V. Casulli, P. Zanolli, Semi-implicit numerical modeling of nonhydrostatic free-surface flows for environmental problems, Math. Comput. Model. 36 (9–10) (Dec. 2002) 1131–1149.
[19] A.J. Chorin, J.E. Marsden, A Mathematical Introduction to Fluid Mechanics, Springer, New York, 1993.
[20] B. Cockburn, C.-W. Shu, The local discontinuous Galerkin method for time-dependent convection-diffusion systems, SIAM J. Numer. Anal. 35 (6) (Dec. 1998) 2440–2463.
[21] A.J.C.B. de Saint-Venant, Théorie du mouvement non permanent des eaux, avec application aux crues des rivières et à l'introduction des marées dans leur lit, C. R. Acad. Sci., Paris 73 (1871) 147–154.
[22] K.D. Devine, J.E. Flaherty, Parallel adaptive *hp*-refinement techniques for conservation laws, Appl. Numer. Math. 20 (4) (Apr. 1996) 367–386.
[23] M. Dumbser, M. Castro, C. Parés, E.F. Toro, ADER schemes on unstructured meshes for non-conservative hyperbolic systems: applications to geophysical flows, Comput. Fluids 38 (2009) 1731–1748.
[24] C. Escalante, M. Dumbser, Manuel J. Castro, An efficient hyperbolic relaxation system for dispersive non-hydrostatic water waves and its solution with high order discontinuous Galerkin schemes, J. Comput. Phys. 394 (2019) 385–416.
[25] C. Escalante, E. Fernández-Nieto, T. Morales de Luna, Manuel J. Castro, An efficient two-layer non-hydrostatic approach for dispersive water waves, J. Sci. Comput. 79 (2019) 273–320.
[26] C. Escalante, T. Morales de Luna, A general non-hydrostatic hyperbolic formulation for Boussinesq dispersive shallow flows and its numerical approximation, J. Sci. Comput. 83 (2020) 62.
[27] E.D. Fernández-Nieto, J. Garres-Díaz, A. Mangeney, G. Narbona-Reina, A multilayer shallow model for dry granular flows with the $\mu(I)$-rheology: application to granular collapse on erodible beds, J. Fluid Mech. 798 (Jun. 2016) 643–681.
[28] E.D. Fernández-Nieto, J. Garres-Díaz, A. Mangeney, G. Narbona-Reina, 2D granular flows with the $\mu(I)$ rheology and side walls friction: a well-balanced multilayer discretization, J. Comput. Phys. 356 (2018) 192–219.
[29] E.D. Fernández-Nieto, E.H. Koné, T. Morales de Luna, R. Bürger, A multilayer shallow water system for polydisperse sedimentation, J. Comput. Phys. 238 (April 2013) 281–314.
[30] E.D. Fernández-Nieto, E.H. Koné, T. Chacón Rebollo, A multilayer method for the hydrostatic Navier-Stokes equations: a particular weak solution, J. Sci. Comput. 60 (2) (Nov. 2013) 408–437.
[31] J. Garres-Díaz, L. Bonaventura, Flexible and efficient discretizations of multilayer models with variable density, Appl. Math. Comput. 402 (Aug. 2021) 126097.

[32] J. Garres-Díaz, F. Bouchut, E.D. Fernández-Nieto, A. Mangeney, G. Narbona-Reina, Multilayer models for shallow two-phase debris flows with dilatancy effects, J. Comput. Phys. 419 (Oct. 2020) 109699.
[33] J. Garres-Díaz, M.J. Castro Díaz, J. Koellermeier, T. Morales de Luna, Shallow water moment models for bedload transport problems, Commun. Comput. Phys. 30 (3) (Jun. 2021) 903–941.
[34] J.-F. Gerbeau, B. Perthame, Derivation of viscous Saint-Venant system for laminar shallow water; numerical validation, Discrete Contin. Dyn. Syst., Ser. B 1 (1) (2001) 89–102.
[35] J.M.N.T. Gray, A.N. Edwards, A depth-averaged $\mu(I)$-rheology for shallow granular free-surface flows, J. Fluid Mech. 755 (Aug. 2014) 503–534.
[36] E. Guerrero Fernández, M.J. Castro-Díaz, T. Morales de Luna, A second-order well-balanced finite volume scheme for the multilayer shallow water model with variable density, Mathematics 8 (5) (2020).
[37] E. Guerrero Fernández, C. Escalante, Manuel J. Castro, Well-balanced high-order discontinuous Galerkin methods for systems of balance laws, Mathematics 10 (1) (2022).
[38] D. Haidvogel, J. Wilkin, R. Young, A semi-spectral primitive equation ocean circulation model using vertical sigma and orthogonal curvilinear horizontal coordinates, J. Comput. Phys. 94 (1) (May 1991) 151–185.
[39] F. Hecht, New development in FreeFem++, J. Numer. Math. 20 (3–4) (2012) 251–265.
[40] A.A. Khan, P.M. Steffler, Vertically averaged and moment equations model for flow over curved beds, J. Hydraul. Eng. 122 (1) (Jan. 1996) 3–9.
[41] J. Koellermeier, Derivation and numerical solution of hyperbolic moment equations for rarefied gas flows, PhD thesis, RWTH Aachen University, July 2017.
[42] J. Koellermeier, M. Rominger, Analysis and numerical simulation of hyperbolic shallow water moment equations, Commun. Comput. Phys. 28 (2020), https://doi.org/10.4208/cicp.OA-2019-0065.
[43] J. Koellermeier, M. Torrilhon, Numerical solution of hyperbolic moment models for the Boltzmann equation, Eur. J. Mech. B, Fluids 64 (July 2017) 41–46.
[44] D.A. Kopriva, G. Gassner, On the quadrature and weak form choices in collocation type discontinuous Galerkin spectral element methods, J. Sci. Comput. 44 (2) (2010) 136–155.
[45] J. Kowalski, M. Torrilhon, Moment approximations and model cascades for shallow flow, Commun. Comput. Phys. 25 (3) (2018) 669–702.
[46] A. Kurganov, G. Petrova, A second-order well-balanced positivity preserving central-upwind scheme for the Saint-Venant system, Commun. Math. Sci. 5 (1) (2007) 133–160.
[47] G. Ma, F. Shi, J.T. Kirby, Shock-capturing non-hydrostatic model for fully dispersive surface wave processes, Ocean Model. 43 (2012) 22–35.
[48] T. Morales de Luna, E.D. Fernández Nieto, M.J. Castro Díaz, Derivation of a multilayer approach to model suspended sediment transport: application to hyperpycnal and hypopycnal plumes, Commun. Comput. Phys. 22 (5) (2017) 1439–1485.
[49] C. Parés, M. Castro, On the well-balance property of Roe's method for nonconservative hyperbolic systems applications to shallow-water systems, ESAIM: Math. Model. Numer. Anal. 38 (5) (Sep. 2004) 821–852.
[50] N.A. Phillips, A coordinate system having some special advantages for numerical forecasting, J. Atmos. Sci. 14 (2) (1957) 184–185.
[51] K.A. Schneider, J.M. Gallardo, C. Escalante, Efficient GPU implementation of multidimensional incomplete Riemann solvers for hyperbolic nonconservative systems: applications to shallow water systems with topography and dry areas, J. Sci. Comput. 92 (2022) 1–42.
[52] P.M. Steffler, J.Y. Chung, Depth averaged and moment equations for moderately shallow free surface flow, J. Hydraul. Res. 31 (1) (Jan. 1993) 5–17.
[53] X. Zhong, C.-W. Shu, A simple weighted essentially nonoscillatory limiter for Runge–Kutta discontinuous Galerkin methods, J. Comput. Phys. 232 (1) (2013) 397–415.